Structure-activity relationship of inositol thiophosphate analogs as allosteric activators of *Clostridioides difficile* toxin B.

Rebecca Cummer, Félix Grosjean, Raphaël Bolteau[1], Seyed Ehsan Vasegh, Simon Veyron, Liam Keogh, Jean-François Trempe, Bastien Castagner*.

Department of Pharmacology and Therapeutics, McGill University, Québec, Canada.

ABSTRACT

Clostridioides difficile is a bacterium that causes life-threatening intestinal infections. Infection symptoms are mediated by a toxin secreted by the bacterium. Toxin pathogenesis is modulated by the intracellular molecule, inositol-hexakisphosphate (IP6). IP6 binds to a cysteine protease domain (CPD) on the toxin, inducing auto-proteolysis, which liberates a virulence factor in the cell cytosol. We developed second-generation IP6 analogs designed to induce auto-proteolysis in the gut lumen, prior to toxin uptake, circumventing pathogenesis. We synthesized a panel of thiophosphate-/sulfate-containing IP6 analogs, and characterized their toxin binding affinity, auto-proteolysis induction and cation interactions. Our top candidate was soluble in extracellular cation concentrations, unlike IP6. The IP6 analogs were more negatively charged than IP6, which improved affinity and stabilization of the CPD, enhancing toxin auto-proteolysis. Our data illustrate the optimization of IP6 with thiophosphate biomimetics which are more capable of inducing toxin auto-proteolysis than the native ligand, warranting further studies *in vivo*.

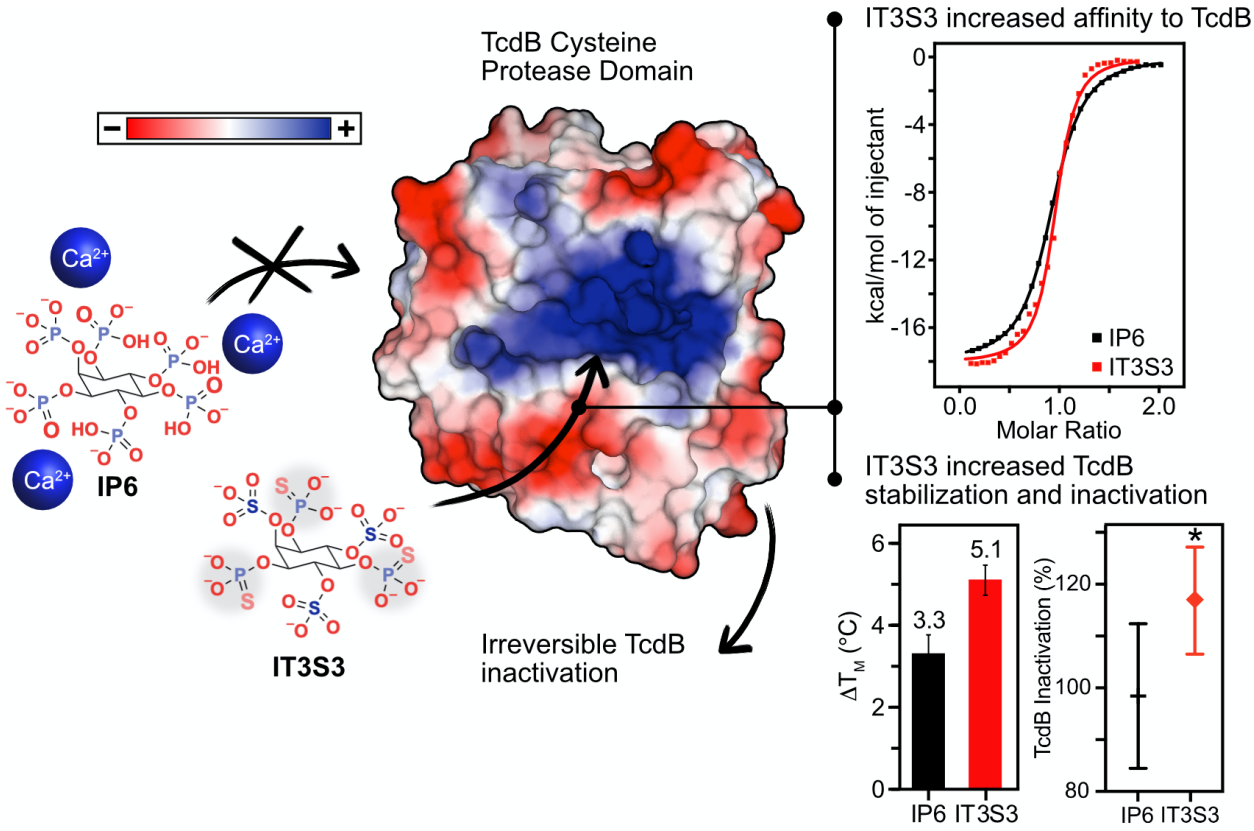

INTRODUCTION

Clostridioides difficile is an anaerobic, spore-forming bacterium that can cause symptoms ranging from diarrhea to life-threatening inflammation of the colon. *C. difficile* infection (CDI) is facilitated by alteration of the microbiome following antibiotic administration, and is prevalent in settings where antibiotics are frequently used.[1,2] In fact, in 2019 the Centers for Disease Control and Prevention (CDC) listed CDI is an urgent antibiotic resistant threat in the United States.[3] First line treatments for CDI typically involve antibiotics, however, antibiotics can lead to high rates of recurrent infection, creating a need for more novel therapeutics.[4] An interesting therapeutic strategy is to block the pathogen's ability to harm the host by inhibiting its virulence factor(s), this would neutralize the pathogenic factor while leaving the microbiome unaltered.[5] The pathogenesis of CDI is mediated by the large clostridial toxins: toxin A (TcdA) and toxin B (TcdB), of which are secreted in the colon lumen.[6,7] Both TcdA and TcdB can cause injuries *in vitro* and in hamsters, but TcdB is the main virulence factor in murine models and human disease.[8,9,10] After binding to epithelial cells via its receptor binding domain, TcdB is endocytosed.[11] Following a pH-dependent conformational change, the cysteine protease domain (CPD) and glucosyltransferase domain (GTD) are translocated to the cytosol. There, intracellular

inositol hexakisphosphate (IP6) binds to the CPD allosteric binding site, inducing auto-proteolysis, liberating the GTD.[12] The freed GTD glucosylates Rho and Rac GTPases to disrupt the actin cytoskeleton, causing cell rounding and ultimately cell death.[13] TcdB is a validated therapeutic target. Bezlotoxumab, a human monoclonal antibody that targets TcdB, has been shown to prevent the recurrence of CDI in conjunction with antibiotics.[8,14] Efforts have also been made to develop small molecules that target TcdB, although none have been FDA approved.[15,16,17,18,19]

IP6 analogs that irreversibly inactivate TcdB in the gut lumen by pre-emptively triggering CPD auto-proteolysis is an attractive therapeutic strategy that showed *in vivo* efficacy in a CDI mouse model.[20] IP6 binds to an allosteric binding site on CPD, initiating interactions with a β-flap region that is coupled to protease activation.[21] IP6 has an unusually high charge density[22] and the CPD allosteric binding site has many basic amino acids that are positively charged at a neutral pH; the resultant electrostatic interactions stabilize the active protease conformation, inducing auto-proteolysis.[21] It is hypothesized that dietary sources of IP6 are incapable of inducing pre-emptive auto-proteolysis in the gastrointestinal (GI) lumen due to its insolubility in the presence of multivalent cations.[23] In fact, IP6 is a known anti-nutrient due to its strong chelative properties which precipitates essential nutrients.[24,25] The first-generation IP6 analogs improved the solubility of IP6 in the presence of calcium by replacing the phosphate groups with sulfates.[20] Akin to IP6, the IP6 analogs are cell impermeable due to the bulky electronegative functional groups, making these small molecules capable of inducing auto-proteolysis in the GI lumen. We aim to pursue this strategy further and design improved IP6 analogs for the treatment of CDI.

We report a structure-activity relationship (SAR) effort that led the development of second-generation IP6 analogs containing thiophosphates and sulfates on the inositol core. Swapping of phosphates for thiophosphates has shown to have advantageous properties in other drug design strategies. For example, thiophosphate analogs have been shown to be resistant to phytase hydrolysis[20,26], improve potency, stabilization[27], binding affinity[28] and substrate kinetics[29] with their target protein, in comparison with their phosphate counterparts. Collectively these results suggest thiophosphate biomimetics are a promising means to improve the pharmacodynamic properties of phosphate containing molecules. Here we carefully control the position and number of thiophosphates on the inositol core to resolve the SAR between the

thiophosphate moieties and the allosteric binding site by assessing our resultant library of small molecules. First, we determined the effect thiophosphates have on IP6 analog solubility and divalent cation chelation, to ensure our analogs maintain allosteric activation in the GI lumen. Second, we characterized the binding interaction between the analogs and TcdB by determining their binding affinity and potency. We found the thiophosphate analogs were soluble in the presence of divalent cations and improved affinity to the CPD and potency for TcdB auto-proteolysis. The improved pharmacodynamic properties were attributed to differences in pK between phosphates and thiophosphates determined via NMR titration curves. The increased charge density of the IP6 analogs improved stabilization of TcdB which caused structural differences in the apo- form as observed via protein NMR. The novel lead IP6 analog, IT3S3, is more capable of inducing TcdB auto-proteolysis than the natural co-factor of the toxin, IP6.

RESULTS AND DISCUSSION

Synthesis.

We synthesized a series of IP6 analogs where the phosphate groups were replaced with a varied ratio of sulfates and thiophosphates, intending to determine the SAR between the thiophosphate containing IP6 analogs and the CPD of TcdB. We synthesized IP6 analogs containing one (IT1S5 and IS5T1), two (IT2S4, previously synthesized[20]), three (IT3S3 and IS3T3), or six (IT6) thiophosphates, where the remaining functional groups were sulfates (Figure 1). We also synthesized two sets of regioisomers, IT1S5/IS5T1 and IT3S3/IS3T3, to determine whether the placement of the thiophosphates on the inositol core altered the functionality of the IP6 analogs.

Synthesis of the inositol orthoformate **1** and orthobenzoate **2** served as starting points for the differentiation of the various inositol derivatives.[30,31] Next, benzyl and/or *para*-methoxy benzyl protective groups were selectively added to differentiate specific free hydroxyl groups for the addition of sulfates in the final step of each synthetic route.[31,32,33] The orthoesters were then deprotected via either a reduction (Na/NH_3 or DIBAL-H) or an acidification (HCl). Thiophosphorylation was performed by a P^{III} method, followed by sulphur oxidation.[34] Thus, the partially protected inositols **3**, **9**, **13**, or **18** were reacted with dibenzyl-*N*,*N*-diisopropyl phosphoramidite and 5-phenyl-1*H*-tetrazole and then oxidized using sulphur in pyridine to afford the fully protected phosphorothioate intermediates **6**, **10**, **14**, and **19**. A complete deprotection of

the benzyl groups was performed with sodium in liquid ammonia.[34] Final sulfation of the free hydroxyl groups in the presence of deprotected phosphate groups proceeded smoothly with sulfur trioxide *N*,*N*-dimethylformamide complex, as previously demonstrated for the synthesis of IT2S4.[20] IT6 was synthesized as reported previously.[35] The compounds were purified via size-exclusion chromatography, and then treated with a cation-exchange resin to ensure compounds **8**, **12**, **16**, and **21** were in their Na^+ form. The concentration of the compounds was determined via ^1H NMR with an internal standard to account for the Na^+ counterions.

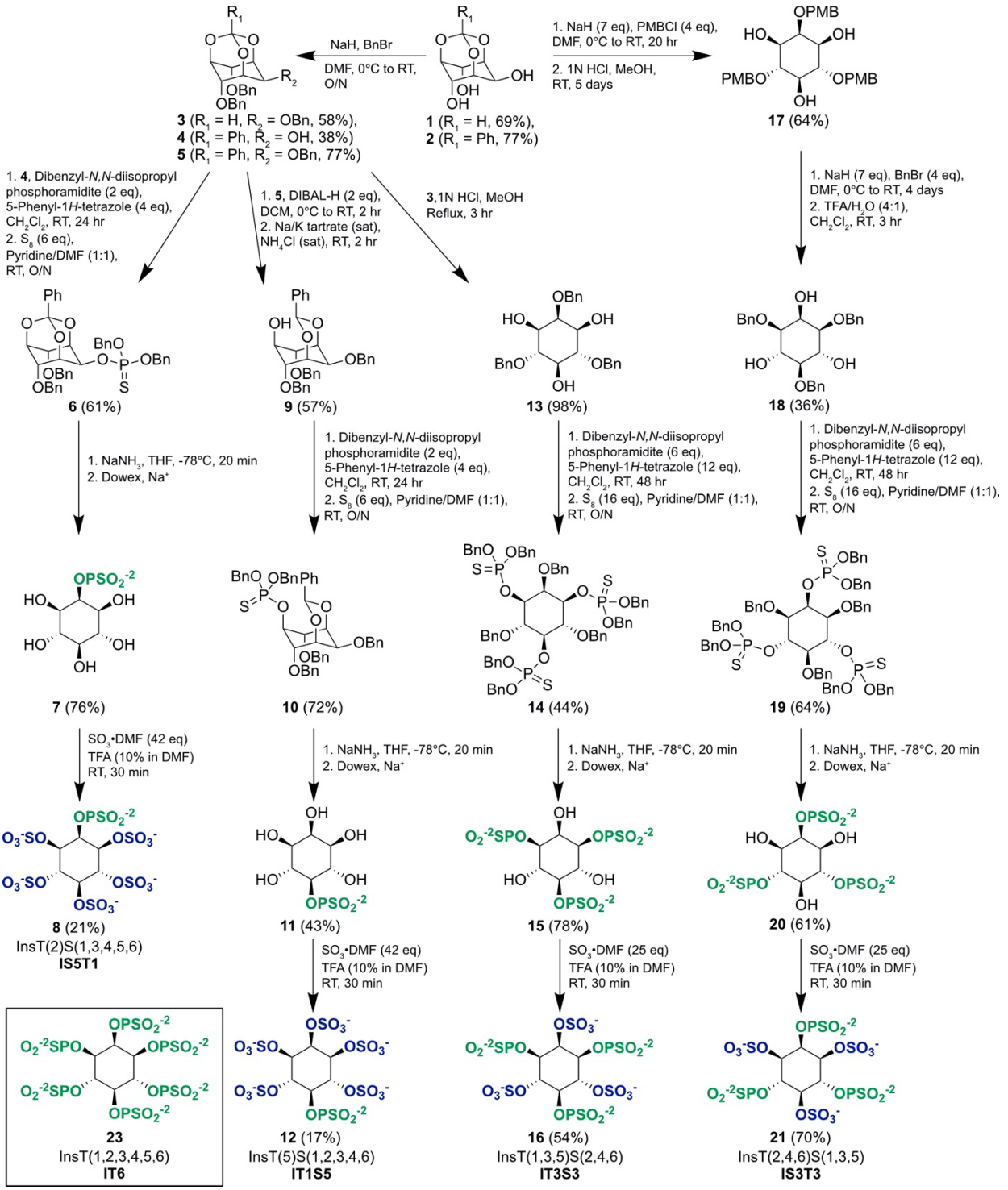

Figure 1. Synthesis of novel inositol thiophosphate and sulfate compounds. Synthesis of IT6 was previously reported.[35] BnBr, benzyl bromide; DMF, dimethylformamide; O/N, overnight; PMBCl, *para*-methoxybenzyl chloride; DIBAL-H, diisobutylaluminum hydride; TFA, trifluoroacetic acid; THF, tetrahydrofuran; SO_3·DMF, sulfur trioxide *N*,*N*-dimethylformamide complex.

Determination of the ability for IP6 analogs to induce TcdB auto-proteolysis.

To test the ability of the IP6 analogs to induce TcdB auto-proteolysis (Figure 2A) we performed an extent cleavage assay to determine the amount of TcdB each IP6 analog can cleave over 3 hr at 37°C. The toxin cleavage was assessed via densitometry measurements from an SDS-PAGE with a silver stain (Figure 2C). First, we found increasing the number of thiophosphates on the inositol core progressively improved extent cleavage (Figure 2D). Maximal TcdB cleavage was observed for IT3S3 with no further improvement by IT6. Previously we found that *myo*-inositol hexasulfate (IS6) was incapable of inducing TcdB cleavage in this context.[20] Interestingly, IT1S5 performed as well as IP6, suggesting that the presence of a single thiophosphate was sufficient to restore activity of IS6. Moreover, the placement of the thiophosphates on the inositol core was important, as both isomer pairs, IT1S5/IS5T1 and IT3S3/IS3T3, showed a significant difference in their ability to induce TcdB cleavage. This finding suggests that despite a pseudosymmetry, the IP6 analogs do not rotate in the CPD allosteric binding site to find an optimal binding position. If the analogs could adopt different binding poses, we would expect no difference in extent cleavage between the isomer pairs. In addition, IT1S5 and IT3S3 both performed better than their respective isomers. Both structures position a thiophosphate on the 5-position of the inositol core, suggesting a potential important interaction between this functional group and its target (*vide infra*).

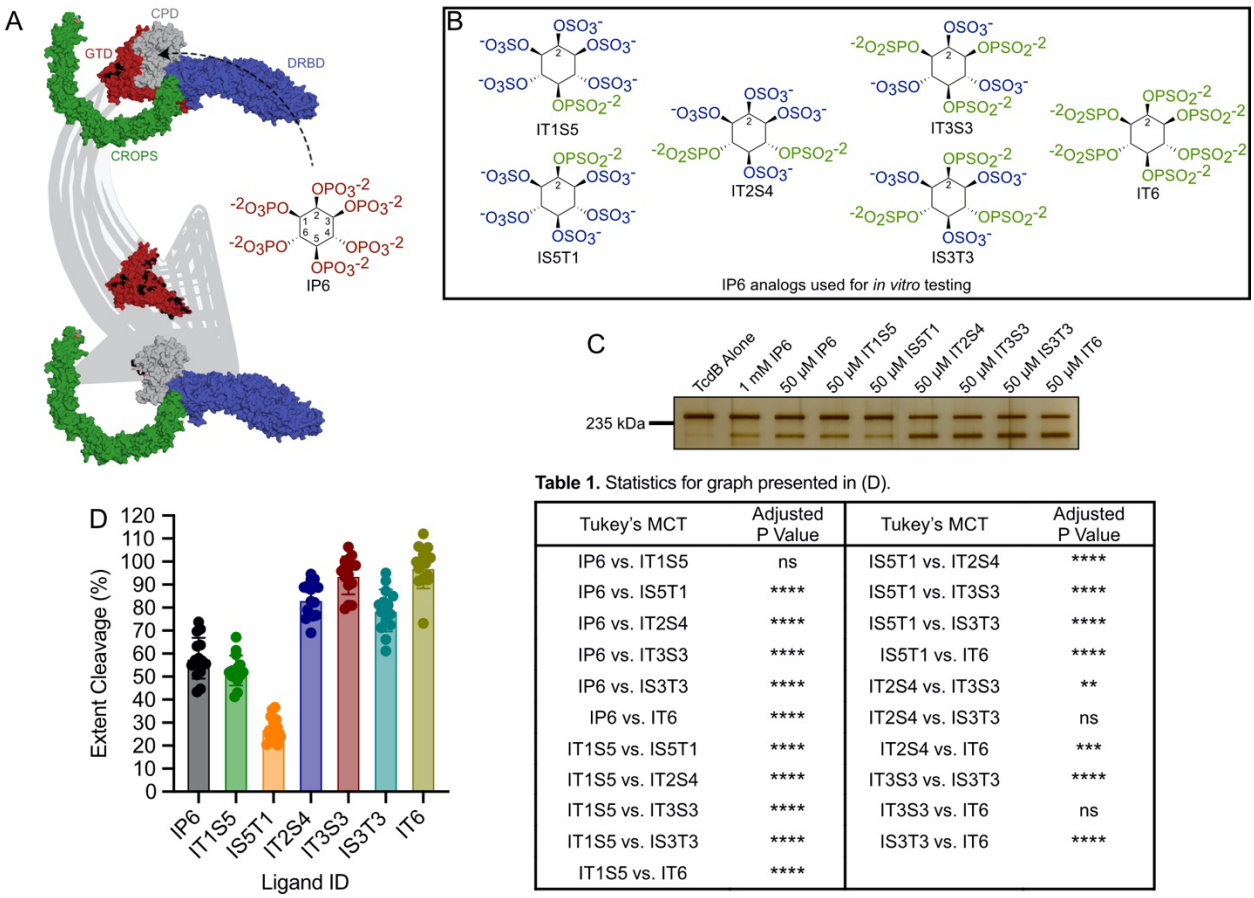

Table 1. Statistics for graph presented in (D).

Tukey's MCT	Adjusted P Value	Tukey's MCT	Adjusted P Value
IP6 vs. IT1S5	ns	IS5T1 vs. IT2S4	****
IP6 vs. IS5T1	****	IS5T1 vs. IT3S3	****
IP6 vs. IT2S4	****	IS5T1 vs. IS3T3	****
IP6 vs. IT3S3	****	IS5T1 vs. IT6	****
IP6 vs. IS3T3	****	IT2S4 vs. IT3S3	**
IP6 vs. IT6	****	IT2S4 vs. IS3T3	ns
IT1S5 vs. IS5T1	****	IT2S4 vs. IT6	***
IT1S5 vs. IT2S4	****	IT3S3 vs. IS3T3	****
IT1S5 vs. IT3S3	****	IT3S3 vs. IT6	ns
IT1S5 vs. IS3T3	****	IS3T3 vs. IT6	****
IT1S5 vs. IT6	****		

Figure 2. Determination of the ability for IP6 analogs to induce TcdB auto-proteolysis, quantified by TcdB extent cleavage (%). (A) IP6 binds to the CPD domain of TcdB which induces auto-proteolysis, liberating the GTD from the toxin. PDB: 6OQ5.[36] (B) Structure and identifier for each of the IP6 analogs tested. IT2S4 was previously synthesized and described.[20] (C) SDS-PAGE with a silver stain of TcdB auto-proteolysis induced by incubation of 150 ng TcdB for 3 hr at 37°C with 1 mM IP6 (positive control), 50 µM of IP6 or analog(s). (D) Percent of TcdB cleaved by 50 µM of IP6, or analog(s) over 3 hr at 37°C. Mean ± SD with data points, n = 15; Tukey's MCT, ns = non-significant, ** $p \leq 0.01$, *** $p \leq 0.001$, **** $p \leq 0.0001$ (Table 1).

Characterization of IP6 analog binding to divalent cations.

Since IP6 cannot effectively induce TcdB cleavage in the presence of divalent cations, we were interested in determining whether the thiophosphate moieties on the inositol core would also interact strongly with divalent cations, hindering their ability to interact with TcdB in the GI tract environment. First, we tested whether the presence of physiologically low and high levels of the common divalent cations: calcium (3 and 10 mM)[37], magnesium (1.25 and 10 mM)[38], and zinc (20 and 100 µM)[39,40] affected the ability of the IP6 analogs to induce extent cleavage (Figure 3A). Low and high levels of calcium and magnesium and high levels of zinc significantly

reduced extent cleavage for all compounds in comparison with the extent cleavage observed in the absence of divalent cations. In the presence of high levels of calcium and magnesium a maximal extent cleavage was reached with IT3S3 (51% and 42%), which was reduced upon additional substitution of sulfates for thiophosphates as observed with IT6 (6% and 23%). High levels of zinc reduced extent cleavage for each ligand to negligible levels, whereas low levels of zinc had a marginal effect on extent cleavage, and the extent cleavage successively increased with a greater number of thiophosphate moieties. To note, the divalent cation concentrations used, particularly zinc, may be over approximations as food-derived macromolecules or low molecular weight ligands may complex the cations, reducing bioaccessiblity.[39] These results indicate that IT3S3 has the optimal ability to induce auto-proteolysis in the presence of calcium and magnesium and that further increasing the number of thiophosphates on the inositol core above three is detrimental.

The extent cleavage assay results are a summation of the differences in the ability for IP6 analogs to induce extent cleavage, and the strength of their interaction with divalent cations. To directly address how the number of thiophosphate moieties effects the binding interaction with divalent cations in the GI tract, we determined whether each of the IP6 analogs precipitates, as observed with IP6, in the presence of low and high concentrations of $CaCl_2$, $MgCl_2$, and $ZnCl_2$ at a pH of 2 – 8 (Figure 3B). EDTA acted as a control as it is a strong chelator of Ca^{2+} and Mg^{2+}.[41] We performed a turbidimetric precipitation assay to qualitatively determine the amount of precipitation observed in the varied solutions. IP6 precipitated out of solution in the presence of low and high concentrations of $CaCl_2$ and $MgCl_2$ at pH's found in the small and large intestines. IS5T1, IT2S4, IT3S3, and IT6 had no detectable precipitate in any of the conditions. The analogs remained soluble in the presence of divalent cations, irrespective of the number of thiophosphate moieties on the inositol core; therefore thiophosphate-containing IP6 analogs do not precipitate in the presence of divalent cations, unlike phosphate-containing IP6 analogs.[20] It is however possible that the IP6 analogs chelate the divalent cations without precipitating.

We tested the chelative properties of IT1S5, IT2S4, IT3S3, and IT6 via a colorimetric assay to determine the amount of free divalent cations in the presence of each of the IP6 analogs. In the presence of 200 μM $CaCl_2$ or $MgCl_2$ all the IP6 analogs decreased the concentration of free cations (Figure 3C). However, in the presence of $CaCl_2$ increasing the number of thiophosphate moieties on the inositol core decreased the concentration of free calcium (Figure

4D). Collectively these results indicate that increasing the number of thiophosphates did not alter the solubility of the ligands, but progressively increased calcium chelation, explaining the need to balance the number of thiophosphates and sulfates on the inositol core necessary to ensure binding to TcdB in physiological conditions.

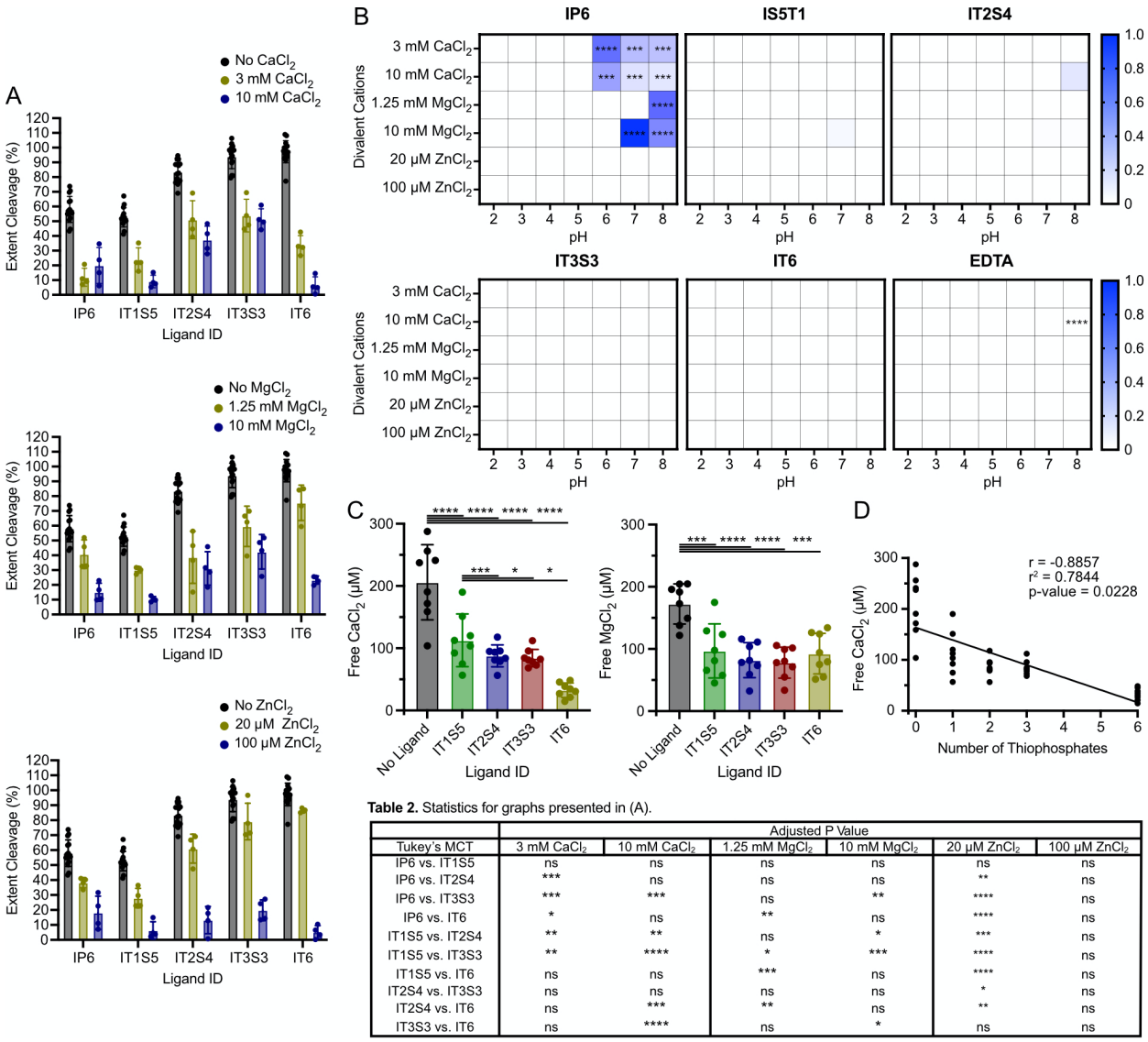

Table 2. Statistics for graphs presented in (A).

	Adjusted P Value					
Tukey's MCT	3 mM $CaCl_2$	10 mM $CaCl_2$	1.25 mM $MgCl_2$	10 mM $MgCl_2$	20 µM $ZnCl_2$	100 µM $ZnCl_2$
IP6 vs. IT1S5	ns	ns	ns	ns	ns	ns
IP6 vs. IT2S4	***	ns	ns	ns	**	ns
IP6 vs. IT3S3	***	***	ns	**	****	ns
IP6 vs. IT6	*	ns	**	ns	****	ns
IT1S5 vs. IT2S4	**	**	ns	*	***	ns
IT1S5 vs. IT3S3	**	****	*	***	****	ns
IT1S5 vs. IT6	ns	ns	***	ns	****	ns
IT2S4 vs. IT3S3	ns	ns	ns	ns	*	ns
IT2S4 vs. IT6	ns	***	**	ns	**	ns
IT3S3 vs. IT6	ns	****	ns	*	ns	ns

Figure 3. Determination of the effect of thiophosphates on the interaction between IP6 analogs and divalent cations. (A) Percent of TcdB cleaved by 50 µM of IP6 or analogs over 3 hr at 37°C in the presence of 3 and 10 mM $CaCl_2$, 1.25 and 10 mM $MgCl_2$, and 20 and 100 µM $ZnCl_2$. Mean ± SD with data points, n = 4; Tukey's MCT, ns = non-significant, * $p \leq 0.05$, ** $p \leq 0.01$, *** $p \leq 0.001$, **** $p \leq 0.0001$ (Table 2). Black bars have no divalent cations present, as originally shown in Figure 2., n = 15. (B) Heat map of the relative precipitation of 250 µM of IP6, IS5T1, IT2S4, IT3S3, IT6, and EDTA at various pH's and in the presence of low and high concentrations of divalent cations (3 and 10 mM $CaCl_2$, 1.25 and 10 mM $MgCl_2$, 20 and 100 µM $ZnCl_2$). Precipitation was measured by a turbidimetric precipitation assay. n = 4; Wilcoxon T-test, *** $p \leq 0.001$, **** $p \leq 0.0001$. (C) Determination of the amount of free $CaCl_2$ or $MgCl_2$ by a

colorimetric assay. 200 μM of IP6 analog, 200 μM of $CaCl_2$ or $MgCl_2$, and 500 μM of calmagite were mixed, incubated, and centrifuged. Absorbance of the supernatant at 550 nm and 539 nm for $CaCl_2$ and $MgCl_2$ was used to determine free calcium and magnesium as an indirect measurement of chelation. Mean ± SD with data points, n = 8; Tukey's MCT, * $p \leq 0.05$, *** $p \leq 0.001$, **** $p \leq 0.0001$. See Figure S1 for standard curve relating calmagite absorbance (Au) with $CaCl_2/MgCl_2$ concentration. (D) Correlation (Pearson r, r) of the number of thiophosphates on the IP6 analogs with the amount of available $CaCl_2$ detected for each IP6 analog. The diagonal line is the simple linear regression.

Characterizing IP6 analog binding to TcdB.

Next, we wanted to test the thermodynamic properties of IP6 analogs binding to TcdB, to further understand the impact of the number and placement of thiophosphates on inducing TcdB auto-proteolysis. The dissociation constant (K_D) of each of the IP6 analogs was determined via isothermal calorimetry (ITC) (Figure 4A-B). Full-length TcdB was not used for this experiment, as the binding event would induce auto-proteolysis, disturbing the ITC measurement. We recombinantly expressed a fragment of TcdB, a truncated CPD (tCPD), which encompassed the CPD but lacked the cleavable N-terminal portion ($TcdB_{544\text{-}797}$). In the absence of calcium, IT3S3 and IT6 had a strong binding interaction with tCPD (662 nM and 184 nM), while IP6, IT1S5, IS5T1, IT2S4, and IS3T3 had moderate binding interactions (≥ 1.36 μM). These results mirror those from the extent cleavage assay. As we increased the number of thiophosphate moieties on the inositol core, we decreased the K_D. In addition, the isomeric pairs had different K_D's, where the analogs with a thiophosphate on the 5-position of the inositol core (IT3S3 and IT1S5) had a significantly higher affinity for tCPD than their isomeric pair. Thus further confirming the importance of the binding interaction between CPD and the 5-position of inositol. In the presence of calcium, IT6, IP6, IT1S5, and IS5T1 did not have a quantifiable binding interaction with tCPD. IT3S3 had the strongest binding interaction (2.66 μM) compared to the other IP6 analogs. These results further suggest that too many thiophosphates on the inositol core prevented IT6 from interacting with CPD due to its strong chelative interaction with Ca^{2+}. While too few thiophosphates prevented IT1S5 and IS5T1 from interacting with CPD, due to a lack of highly electronegative isosteres. These results further confirm that thiophosphates have a stronger binding interaction with CPD than phosphates, however a balance in the number of thiophosphates and sulphates is necessary to ensure accessibility to CPD to avoid cation complexation.

The effective median concentration (EC_{50}) of IP6, IT2S4, IT3S3, and IT6 was determined by the extent cleavage assay in the absence and presence of $CaCl_2$, $MgCl_2$, and $ZnCl_2$. The toxin cleavage was quantified via densitometry measurements from a western blot, and the resultant dose-response curves were fitted to determine the EC_{50} (Figure 4C). IT3S3 and IT6 had the lowest EC_{50}'s in the absence of divalent cations (3.56 and 2.31 μM); however, in the presence of $CaCl_2$, $MgCl_2$, and $ZnCl_2$, IT3S3 had a substantially lower EC_{50} (113 μM) than IT6, IP6, and IT2S4 (≥536 μM). Therefore, less IT3S3 was required to induce TcdB auto-proteolysis in a physiologically relevant environment when compared to IP6 and the IP6 analogs. Interestingly, the EC_{50} results also indicated a difference in efficacy of the small molecules, as the maximal extent cleavage was higher for IT3S3 (117%) than IP6 (98%) (Figure 4D). To note, there is a discrepancy between the quantified K_D and EC_{50} values for each of the compounds. This discrepancy can be attributed to the use of tCPD versus TcdB, as TcdB is a large, dynamic, multi-domain protein which has a less accessible allosteric binding site than tCPD.[11,36]

To gain further insight into the binding pose of IP6 and analogs we determined the crystal structure of tCPD bound to IP6 (PDB 9BJA) at 2.1 Å resolution with molecular replacement using the previous structure of tCPD as a search model (Table 4, align RMSD = 0.297).[21] Co-crystallization of tCPD with analogs were pursued under similar conditions although no diffraction quality crystals were formed. Conditions were also culled with crystallization screens, although no usable hits were found. As a result, we modeled in the structure of IT1S5 and IS5T1, assuming a similar pose to that of IP6 in order to gain insight as to why the placement of the thiophosphate on the 5-position of the inositol core improved the efficacy of the IP6 analog's ability to induce TcdB auto-proteolysis. The thiophosphate on IS5T1 is solvent facing, while the thiophosphate on IT1S5 is buried in the allosteric binding site, interacting with Lys57 and Arg209. Shen *et al.* previously performed site-directed mutagenesis on amino acids directly interacting with IP6 in the allosteric binding site, and determined which amino acids were linked to formation of the CPD active site.[21] Both Lys57 and Arg209 were found to play important roles in the formation of the CPD active site, which corresponded with the cleavage of TcdB. In addition, to validate there are no meaningful interactions between the functional group on the inositol carbon 2-position and CPD, we tested the extent cleavage of IP6 versus 1,3,4,5,6-phosphate-2-*O*-benzyl-*myo*-inositol (IP5Bn), where a non-polar, bulky benzyl group was attached to the 2-position of IP5 (Figure S3). We found there was no significant difference in

extent cleavage induced by IP6 and IP5Bn, confirming that position 2 does not contribute meaningfully to binding and allosteric activation and further validating the model suggested in Figure 4F.

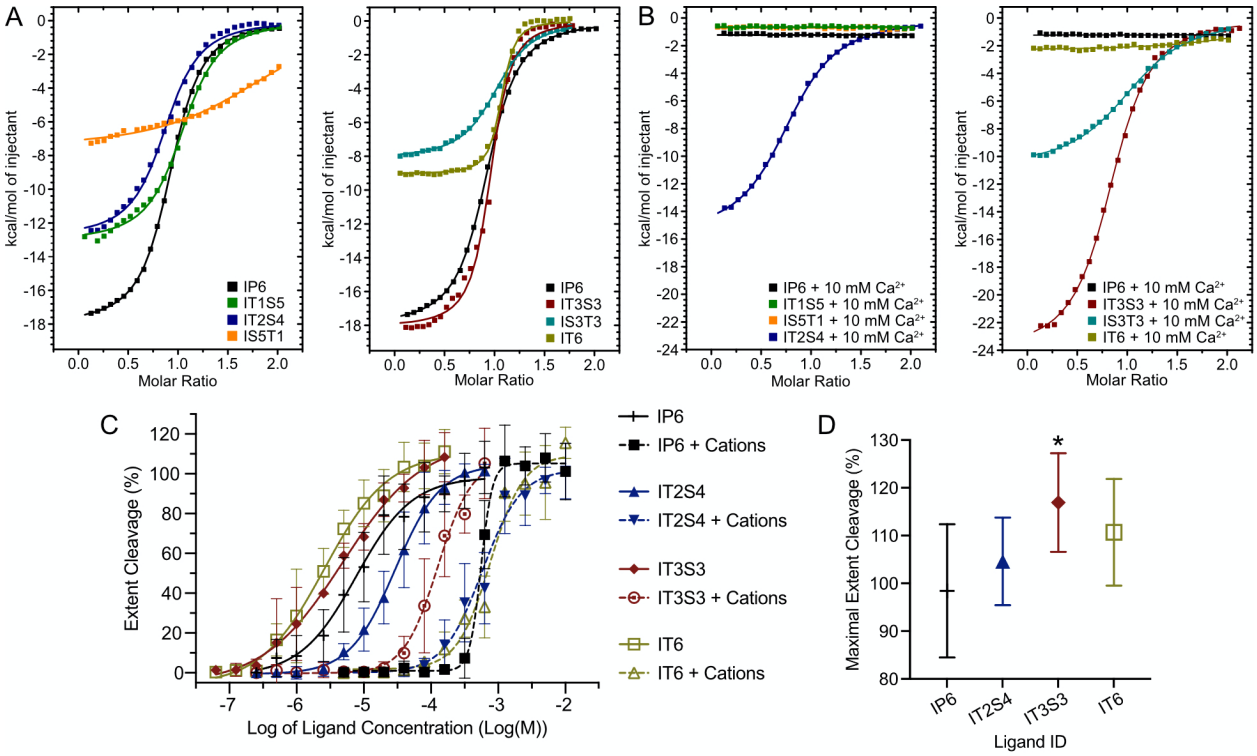

E **Table 3.** K_D and EC_{50} results for graphs presented in (A-C).

Ligand ID	K_D (SD)	K_D + 10 mM Ca^{2+} (SD)	EC_{50} (SD)	EC_{50} + Ca/Mg/Zn (SD)
IP6	1.36 (1.34, 1.38) µM	ND	8.39 (13.77) µM	536 (9.87) µM
IT1S5	2.19 (2.00, 2.43) µM	ND	-	-
IS5T1	7.14 (6.81, 7.51) µM	ND	-	-
IT2S4	2.20 (2.01, 2.42) µM	4.69 (4.58, 4.82) µM	27.1 (9.87) µM	557 (12.26) µM
IT3S3	0.662 (0.609, 0.726) µM	2.66 (2.57, 2.76) µM	3.56 (10.91) µM	113 (11.06) µM
IS3T3	2.26 (2.09, 2.46) µM	5.37 (5.12, 5.66) µM	-	-
IT6	0.184 (165, 208) µM	ND	2.31 (11.66) µM	657 (12.5) µM

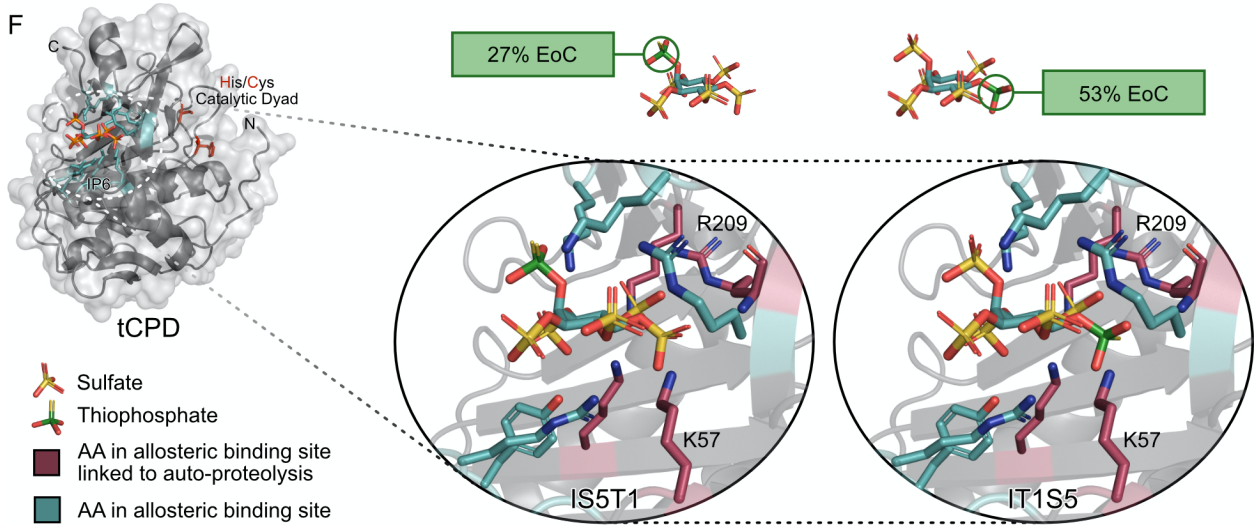

Figure 4. Characterization of the thermodynamic properties of the IP6 analogs binding to TcdB. (A) ITC thermograms of tCPD bound to IP6 and analogs in 10 mM tris, 150 mM NaCl, 1 mM TCEP, pH 7.5. Curves were fit in the Origin software using a one-site model curve fit to determine the dissociation constant (K_D). Errors were derived from fitting statistics. See **S2** for raw data set. (B) ITC thermograms of tCPD bound to IP6 and analogs in 10 mM tris, 150 mM NaCl, 1 mM TCEP, pH 7.5 with 10 mM $CaCl_2$. Curves were fitted in the Origin software using a one-site model curve fit to determine the K_D. Errors are derived from fitting statistics. (C) Dose-response curves for the determination of the EC_{50} of IP6, IT2S4, IT3S3, and IT6 in the absence or presence of divalent cations. Percent of TcdB cleaved by a serial dilution of IP6 or analogs over 3 hr at 37°C in the absence and presence of 1 mM $CaCl_2$, 150 µM $MgCl_2$, and 12 µM $ZnCl_2$ was plotted. The data were fitted with a nonlinear curve fit. Mean ± SD; n = 6. (D) Maximal percentage of TcdB cleaved, set to a positive control of 1 mM IP6. Percent cleavage above 100% indicates more cleavage was observed than the positive control. Mean ± SD, n = 6; Tukey's MCT, * $p \leq 0.05$. (E) Summary table showing the calculated K_D and EC_{50} values for the IP6 analogs with tCPD or TcdB, respectively. (F) Model of IT1S5 and IS5T1 binding pose in tCPD based on IP6 binding (PDB 9BJA).

pK determination and net proton change upon tCPD binding.

Next, we wanted to understand why the thiophosphate containing analogs showed an improved affinity and efficacy for the CPD allosteric binding site and a higher potency for auto-proteolysis than the natural co-factor IP6. Previous literature has left conflicting explanations as to why thiophosphate analogs have an improved thermodynamic profile when compared with the respective phosphate-containing compounds.[27,35,42] It was suggested that thiophosphate analogs maintain an amphipathic character due to a desolvation advantage of sulfur over oxygen, potentially permitting hydrophobic interactions within a binding site.[42] Alternatively, it was suggested the thiophosphate sulfur has a stronger hydrogen bonding potential than the phosphate oxygen, which effectively eliminates competitive interference with water, permitting more polar interactions with the binding site.[35] It has also been reported that the pK of a lone phosphate is 6.7, while that of a thiophosphate is 5.4.[43] Such a difference in pK could explain an improved K_D for a highly positively charged binding site due to a difference in net charge. Therefore, we determined the pK's of IT6 and IP6 to compare the pK of the thiophosphates and phosphates at each position on the inositol core.

We performed a ^{31}P NMR (with ^{1}H coupling) titration to determine the pK of IP6's phosphates, as described previously (Figure 5A).[22] We explored a pH range of 4-10 which was above the pK values for the diprotic to monoprotic form of each of the phosphate groups.[22] The pK for the phosphates attached to carbons 3, 4, and 6 on the inositol core were not determined as

they fell above the experimental range. The pK's of the remaining phosphates were determined and fell within 0.2 units of the literature values (P1 – 5.96 (*5.70*), P2 – 6.79 (*6.85*), P3 – 7.64 (*7.60*)).[22] Using the same methodology, we determined the monoprotic to dianionic pK of each thiophosphate on IT6. We were surprised to find that IT6 had a substantially lower pK for most of its thiophosphate groups, ranging from 5.47 to 6.63 (Figure 5B). These results suggest that at a pH of 7.5 all the thiophosphates on IT6 are in their dianionic form, unlike IP6. Therefore, IT6 has a greater net charge than IP6 at a physiologically relevant pH. The increased net charge could explain the improved solubility of the IP6 analogs in the presence of divalent cations due to a higher electroneutrality threshold point.[44]

Next, we wanted to test whether IP6 or the IP6 analogs lost a proton at a pH of 7.5 when binding to CPD, due to some of the functional groups having a pK near this pH. We tested the potential coupling of a protonation event with the tCPD binding event using ITC in buffers with different heat of enthalpies, as described previously.[45] We found that IP6 lost 1.28 protons per binding interaction, while IT2S4, IT3S3, and IS3T3 did not have a significant gain or loss of protons during the binding event (Figure 5C). Loss of a ligand proton incurred by a protein is a rare occurrence at a neutral pH due to the energy compromising nature of the event.[46] Collectively these results indicate that the thiophosphate containing compounds are more negatively charged and resistant to the energy compromising protein-induced deprotonation at pH 7.5, further bolstering the IP6 analogs as superior ligands to IP6. These results also explain the improved thermodynamics of IT3S3 and IT6 in comparison with IP6.

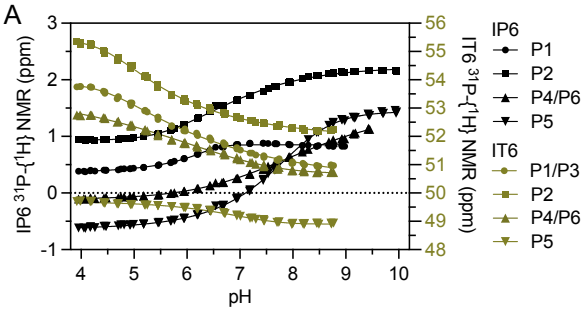

B

Table 4. pK of each phosphorus containing group on IP6 and IT6.

Phosphorus Position	IP6 pK	IT6 pK
P1	5.96 ± 0.01	6.01 ± 0.20
P2	6.79 ± 0.01	5.54 ± 0.06
P3	*	6.01 ± 0.20
P4/P6	*	5.47 ± 0.12
P5	7.64 ± 0.02	6.63 ± 0.02

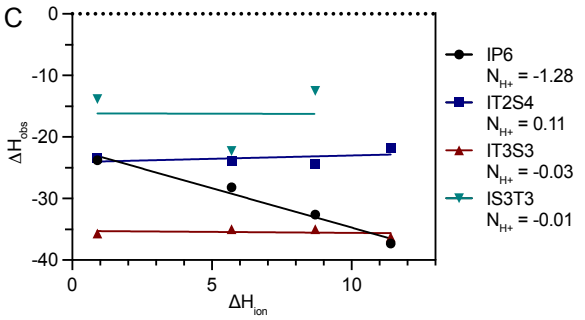

Figure 5. pK determination of IP6 and IT6 and quantification of net proton change upon IP6 analogs binding to tCPD at pH 7.5. (A) ^{31}P NMR (with ^{1}H coupling) titration curves of IP6 (black) and IT6 (gold) for each phosphorus on the inositol core (P1-6). The titration curves were determined between pH 4 to 10, which corresponds with the pK for the monoprotic to dianionic form of most of the phosphorus-containing functional groups. Three replicates were performed for each titration curve, all data points are presented, and have an asymmetric sigmoidal non-linear curve fit. Note: The ppm of each phosphorus in IT6 could not be reliably determined above pH 8.75 due to peak broadening, data points above this pH were excluded. See also Figure S8 and S9. (B) Macroscopic pK determined for the monoprotic to dianionic form of each phosphate on IP6 and IT6. Mean ± SD, n = 3. *Indicates the pK is above the experimental range of pH 4-10. (C) Enthalpy change of binding, ΔH_{obs}, of tCPD to IP6, IT2S4, IT3S3, and IS3T3, as a function of the ionization enthalpy, ΔH_{ion}, of the respective buffers at pH 7.5. The solid lines represent linear least-square fitting of these points. The change in number of bound protons per binding interaction (N_{H+}) is given by the slope. See also Figure S4-S7.

Stabilization and structural changes.

Next, we wanted to determine whether the greater charge density of the thiophosphate containing compounds induced a greater stabilization of tCPD. To test this, we performed a differential scanning fluorimetry (DSF) experiment to determine the melting temperature (T_M) of tCPD alone and in the presence of serial dilutions of IP6, IT1S5, IT2S4, IT3S3, and IT6. From

this we determined the change in melting temperature (ΔT_M) for each ligand concentration when compared to the T_M of tCPD alone (Figure 6A). We then performed a non-linear curve fit on the data set and calculated the maximal ΔT_M for each ligand (Figure 6B). IT2S4, IT3S3, and IT6 had a significant increase in ΔT_M (5.3, 5.1, 5.6°C) while the ΔT_M was comparable for IP6 and IT1S5 (3.3, 3.1°C). These results confirm that the analogs with a higher net charge were more capable of stabilizing tCPD than the natural co-factor IP6.

Following this, we wanted to see whether there were notable structural changes that corresponded with the increased stabilization of IT3S3 when compared to IP6. To test this, we performed a ^{1}H-^{15}N-HSQC NMR experiment of ^{15}N-enriched tCPD alone and in the presence of a molar equivalent of IP6 or IT3S3. We looked at the number of detectable peaks (Figure 6D and Figure S10) to infer the extent of protein immobilization in the active conformer, and we calculated the change in chemical shift of number-matched peak pairs (chemical shift perturbation (CSP) $\Delta\Delta\delta$ ppm) to quantify whether there were significant structural differences between two overlapped spectra.[47] tCPD contains 260 backbone N-H pairs and we only observe 141 peaks in apo-tCPD, likely as a result of exchange broadening in the ligand binding site. Indeed, upon addition of IP6 or IT3S3, the number of peaks increased to 193 and 208 respectively, as a result of stabilization in the binding site (see Figure S10). These results corroborate those from the DSF experiment; IP6 and IT3S3 both stabilized tCPD whereas IT3S3 had a greater stabilization affect than IP6. To note, CSP scores were not calculated for the apo- and holo-tCPD due to unreliable peak numbering from the drastic differences between the HSQC spectra. Next, the holo-tCPD HSQC spectra were superposed for both IP6 and IT3S3 to determine the CSP for each unassigned peak pair (Figure 6C). We found that 49% of the peaks had a significant change in CSP, indicating there was a global structural change that corresponded with the enhanced stabilization of tCPD induced by IT3S3. Finally, we performed a competition assay with equimolar tCPD, IP6, and IT3S3 to determine whether tCPD preferentially bound to IP6 or IT3S3. The resultant HSQC NMR spectrum was superposed with that of IP6-tCPD (Figure S11B) or IT3S3-tCPD (Figure S11A) and a CSP value was calculated for each number-matched peak pair (Figure S12). When the spectrum was superposed with that of IP6-tCPD, 47% of the peak pairs had a significant change and when superposed with that of IT3S3-tCPD, 7% of the peak pairs had a significant change. Therefore, the HSQC spectrum from the competition assay was very similar to that of IT3S3, indicating IT3S3 successfully

outcompetes IP6 to bind tCPD. In addition, a ^{31}P NMR was performed on the competition assay sample (Figure S13) which confirmed IP6 was free while IT3S3 was bound to tCPD. Therefore, the improved thermodynamic properties of IT3S3 allows it to outcompete IP6 for the tCPD allosteric binding site.

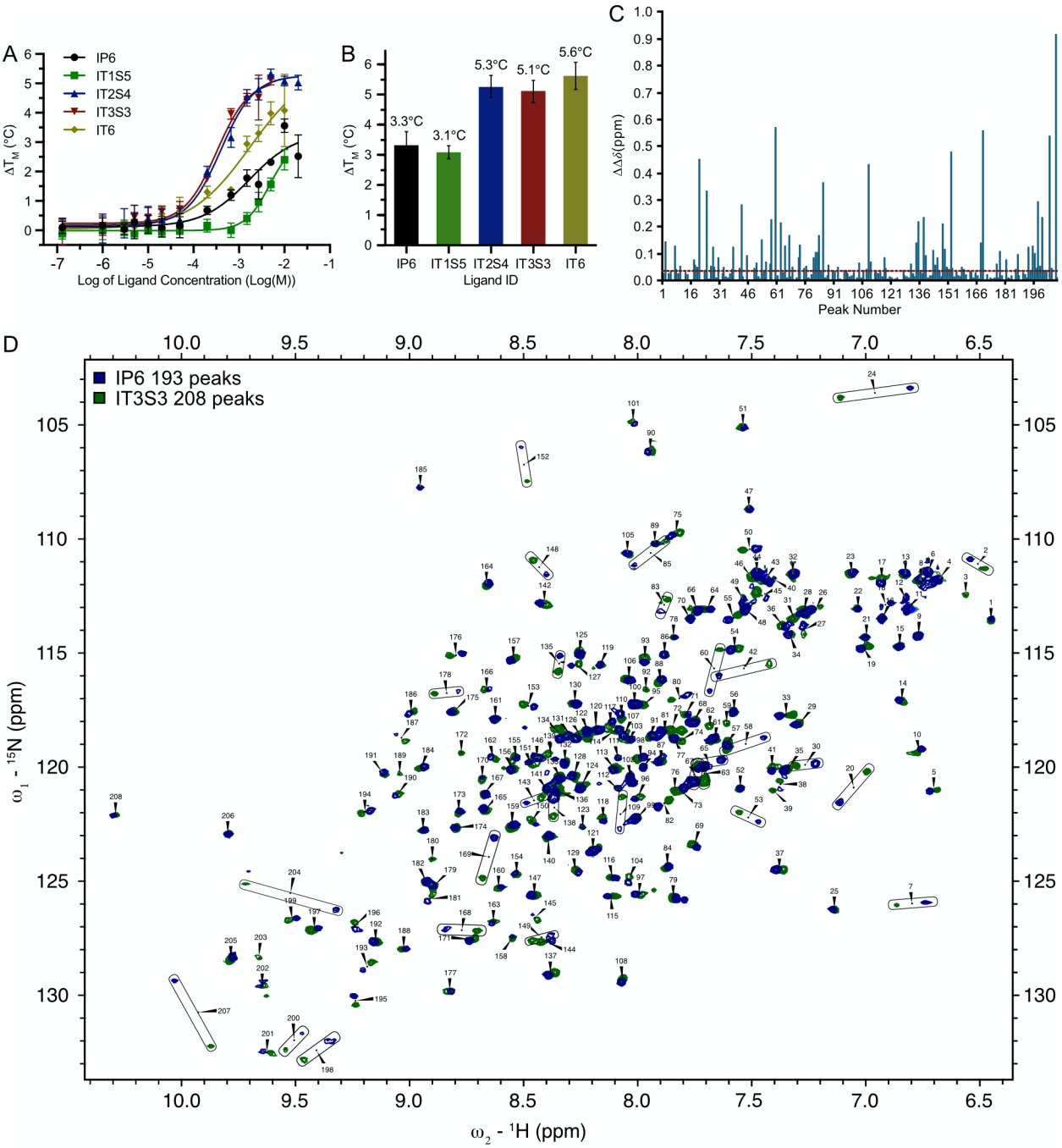

Figure 6. Stabilization and structural changes incurred by the increased net charge of the thiophosphate containing analogs. (A) Dose-response curves for binding of IP6, IT1S5, IT2S4, IT3S3, and IT6 with tCPD and the correspondent temperature stabilization. Stabilization of tCPD was determined via Differential Scanning Fluorometry. The melting temperature (T_M) was

determined for tCPD alone and tCPD in the presence of a serial dilution of IP6 analogs. The difference in melting temperature (ΔT_M) was then plotted and the data were fit with a nonlinear curve fit. Mean ± SD; n = 6. (B) Maximal change in T_M (°C) for IP6, IT1S5, IT2S4, IT3S3, and IT6, as determined in (A). Mean ± SD, n = 6. (C) Quantification of the change in chemical shift, Chemical Shift Perturbation (CPS, $\Delta\Delta\delta$), of matched peaks corresponding to holo-tCPD (350 μM) bound to a molar equivalent of IP6 (350 μM) or a molar equivalent of IT3S3 (350 μM) at pH 7.5. See (D) for data set. The dashed line indicates the 95% threshold (θ) for the variability between two holo-tCPD HSQC bound to the same ligand. Values above θ are noted to have a significant CSP. 49% of the tCPD residues exceeded θ. (D) Two overlapping ^{1}H-^{15}N-HSQC NMR spectra generated from holo-tCPD (350 μM) bound to a molar equivalent of IT3S3 (350 μM, peaks shown in green) or IP6 (350 μM, peaks shown in blue). Peak assignment was made based on the peaks closest together and assignment went from 1 to 208, where 1 was the peak with the lowest ppm on the ^{1}H spectrum and 208 was the peak with the highest ppm. See also Figure S10, S11, and S12.

CONCLUSION

Here we propose IT3S3 as our second-generation lead compound to inactivate *C. difficile* TcdB by pre-emptively inducing auto-proteolysis in the presence of physiologically relevant concentrations of divalent cations. We optimized the IP6 analogs by replacing phosphates with thiophosphates and sulfates. We then determined how the thiophosphates affected the IP6 analog solubility in the presence of divalent cations, and the efficacy of the compounds to induce TcdB auto-proteolysis. We found that the number of thiophosphates on the inositol core needed to be tempered with sulfates to avoid strong chelation with cations present in the GI lumen. Surprisingly, addition of thiophosphates to the inositol core improved the affinity and potency of the analogs for the TcdB CPD beyond that of the natural co-factor IP6. These improved thermodynamic properties can be attributed to the lower pK of the thiophosphate groups on the inositol core, resulting in a greater net charge of the small molecules at a pH of 7.5. As the net charge of the compounds increased above -7, as observed with IT2S4, IT3S3, and IT6, this resulted in a drastic stabilization of tCPD, which had a resultant global structural modification. We hypothesize that the improved stabilization of CPD restrains the conformational dynamics in the active conformer, promoting the activation of the allosteric circuit; thus, causing IT3S3 to induce TcdB auto-proteolysis more effectively than IP6. The second-generation IP6 analog, IT3S3, is a product of the simultaneous optimization of improved binding properties and reduced cation interference. We are currently pursuing the preclinical testing of IT3S3 as a small molecule therapeutic against CDI. In addition, the decreased pK of the thiophosphate-containing analogs and concomitant increased affinity to basic proteins suggest that these bioisosteres could

be useful in the context of other phosphate-binding proteins, both as research tools and/or therapeutics.

EXPERIMENTAL SECTION

Methods and General Procedures

Reagents

Reagent or Resource	Source	Identifier
Biological Samples		
BL21(DE3)	New England Biolabs	Cat# C2527H
pET22b-TcdB$_{543-799}$	Dr. Matthew Bogyo	Stanford University
Native *C. difficile* toxin B	abcam	Cat# ab124001
Chemicals for In Vitro Testing		
Acrylamide/Bis-Acrylamide 30%	BioShop Canada Inc.	Cat# ACR009
Ammonium Chloride (^{15}N, 99%)	Cambridge Isotope Laboratories, Inc.	CAS No. 39466-62-1
Ammonium Citrate Dibasic	Sigma-Aldrich	Cat# 25102
Ammonium Persulfate	Sigma-Aldrich	Cat# 248614
Biotin	Sigma-Aldrich	CAS No. 58-85-5
Bis Tris	BioShop Canada Inc.	CAS No. 6976-37-0
Boric Acid	Sigma-Aldrich	CAS No. 10043-35-3
Calcium Chloride	Fisher Scientific	Cat# BP510500
Calmagite	Sigma-Aldrich	Cat# C204-10G-A
Cobalt Chloride Hexahydrate	BioShop Canada Inc.	Cat# COB001
Copper (II) Sulfate Pentahydrate	Sigma-Aldrich	CAS No. 7758-99-8
D-Glucose	BioShop Canada Inc.	Cat# GLU601
Ethylenediaminetetraacetic Acid (EDTA)	BioShop Canada Inc.	CAS No. 6381-92-6
Ferrous Sulfate Heptahydrate	BioShop Canada Inc.	Cat# FER005
Formaldehyde, 37% by weight	Sigma-Aldrich	Cat# F8775-25ML
Glycerol	Sigma-Aldrich	Cat# G2025
HEPES Sodium	Sigma-Aldrich	Cat# H7006-500G
HisPur Ni-NTA Resin	ThermoFisher Scientific	Cat# PI88221
Imidazole	Fisher Scientific	Cat# O3196
Isopropyl β-D-1-thiogalactopyranoside (IPTG)	Fisher Scientific	CAS No. 367-83-1
Magnesium Chloride Hexahydrate	BioShop Canada Inc.	Cat# MAG510
Manganese Sulfate	BioShop Canada Inc.	Cat# MAG511
2-(N-morpholino)	BioShop Canada Inc.	Cat# MES503

ethanesulfonic acid (MES)		
MOPS	BioShop Canada Inc.	Cat# MOP005.500
Pierce ECL Western Blotting Substrate	ThermoFisher Scientific	Cat# 32209
Potassium Phosphate Monobasic	BioShop Canada Inc.	Cat# PPM302
Potassium Phosphate Dibasic	BioShop Canada Inc.	Cat# PPD303
Reagent or Resource	Source	Identifier
Silver Nitrate	Millipore Sigma	Cat# S-8157
Sodium Acetate Trihydrate	BioShop Canada Inc.	Cat# SAA555.1
Sodium Chloride	BioShop Canada Inc.	Cat# SOD002
Sodium Dodecyl Sulfate	BioShop Canada Inc.	CAS No. 151-21-3
Sodium Phosphate Monobasic	BioShop Canada Inc.	Cat# SPM400
Sodium Thiosulfate	ACP Chemicals	Cat# S-5662
SYPRO Orange Protein Gel Stain	Invitrogen	Cat# S6650
Tetramethylethylenediamine (TEMED)	BioShop Canada Inc.	Cat# TEM001
Tetrabutylammonium Hydroxide, ~1.5 M	Sigma-Aldrich	Cat# 86880-100ML
Thiamine-HCl	BioShop Canada Inc.	Cat# THA001
Tris(2-carboxyethyl) phosphine (TCEP)	Sigma-Aldrich	CAS No. 51805-45-9
Tryptone	BioShop Canada Inc.	Cat# TRP402.500
Tween 20	Sigma-Aldrich	Cat# P1379-100ML
UltraPure Tris	Invitrogen	CAS No. 77-86-1
Yeast Extract	BioShop Canada Inc.	Cat# YEX401.500
Zinc Chloride	BioShop Canada Inc.	Cat#ZNC222
Chemicals for Synthesis		
1H-Tetrazole, 0.45 M in acetonitrile	Alfa Aesar/Johnson Matthey	CAS No. 288-94-8
4-Methoxybenzyl Chloride	Sigma-Aldrich	Cat# 270245
5-Phenyl-*1H*-Tetrazole	Alfa Aesar/Johnson Matthey	Cat# B25664
Acetic Anhydride	Sigma-Aldrich	Cat# 320102-1L
Ammonium Chloride	Sigma-Aldrich	Cat# 213330-500G
Benzyl Bromide	Sigma-Aldrich	Cat# B17905-25G
Camphor-10-sulfonic acid	Sigma-Aldrich	CAS No. 5872-08-2
Carbon Disulfide	Sigma-Aldrich	Cat# 180173-500ML
Cyclohexane	Fisher Scientific	CAS No. 110-82-7
Dibenzyl-*N*,*N*-diisopropyl phosphoramidite	Sigma-Aldrich	Cat# 416436-5ML
Dichloromethane	Sigma-Aldrich	CAS No. 75-09-2
Diethyl Ether, Anhydrous	Fisher Scientific	CAS No. 60-49-7
Diisobutylammonium	Sigma-Aldrich	CAS No. 1191-15-7

Hydride Solution, 1.0 M in Toluene		
N,*N*-Dimethylformamide (DMF), Anhydrous	Acros Organics N.V.	CAS No. 68-12-2
Dimethyl sulfoxide (DMSO), Anhydrous	Fisher Scientific	CAS No. 67-68-5
Reagent or Resource	Source	Identifier
Dowex 50WX8, 50-100 mesh, ion-exchange resin	Fisher Scientific	Cat# AC335331000
Ethyl Acetate	Fisher Scientific	CAS No. 141-78-6
Hexanes	Fisher Scientific	CAS No. 110-54-3
Hydrochloric Acid	Fisher Scientific	Cat# A144S-500
Magnesium Sulfate Anhydrous	Fisher Scientific	Cat# MAG511
Methanol, Anhydrous	Sigma-Aldrich	CAS No. 67-56-1
Myo-inositol	Sigma-Aldrich	Cat# I5125
Potassium Sodium L-(+)-Tartrate Tetrahydrate	TCI America	CAS No. 6381-59-5
Pyridine	Sigma-Aldrich	Cat# 270970
Sephadex LH-20	Sigma-Aldrich	Cat# LH20100
Silica	Sigma-Aldrich	CAS No. 112926-00-8
Sodium, in kerosene	Sigma-Aldrich	CAS No. 7440-23-5
Sodium Bicarbonate	BioShop Canada	Cat# SOB308.5
Sodium Hydride, 60% dispersion in mineral oil	Sigma-Aldrich	Cat# 452912
Sodium Hydroxide	Fisher Scientific	Cat# S318-500
Sodium Methoxide	Sigma-Aldrich	CAS No. 124-41-4
Sulfur	Sigma-Aldrich	CAS No. 7704-34-9
Sulphur Trioxide	Sigma-Aldrich	CAS No. 7446-11-9
Tetrahydrofuran (THF), Anhydrous	Acros Organics N.V.	CAS No. 109-99-9
p-Toluenesulfonic Acid Monohydrate	Sigma-Aldrich	Cat# 402885-100G
Triethylamine	Sigma-Aldrich	Cat# T0886-100ML
Triethyl Orthoformate, Anhydrous	Sigma-Aldrich	CAS No. 122-51-0
Trifluoroacetic Acid	Sigma-Aldrich	Cat# T6508-100ML
Trimethyl orthobenzoate	Sigma-Aldrich	Cat# 164534-50G
Software and Algorithms		
OriginPro	OriginLab	https://www.originlab.com/origin
Prism 10	GraphPad Software	https://www.graphpad.com/
ImageJ	NIH	https://imagej.net/ij/download.html
Mnova	Mestrelab Research	https://mestrelab.com

PyMOL 2.5	Schrödinger	https://pymol.org/2/
TopSpin 4.3.0	Bruker	https://bruker.com/en.html
POKY	University of Colorado, Denver	https://doi.org/10.1093/bioinformatics/btab180

Characterization of Compounds

NMR spectra were recorded on AVIIIHD 500 or 600 MHz Bruker spectrometers and a Varian Inova QUANC 400 or 500 MHz. The spectra were calibrated to the residual ^{1}H and ^{13}C signals of the solvents. Chemical shifts are reported in ppm. Multiplicities are abbreviated as follows: singlet (s), doublet (d), triplet (t), quartet (q), septet (sept), doublet-doublet (dd), doublet-triplet (dt), doublet-quartet (dq), triplet-doublet (td), multiplet (m), and broad signal (br s). High resolution electrospray ionization mass spectrometry, HRMS (ESI), were obtained on a Thermo Exactive Plus Orbitrap or a Bruker Maxis Impact QTOF. The purity of the compounds was assessed via NMR as the high polarity and lack of chromophore of the compounds rendered them unsuitable for an LC-MS purity assessment. The concentration of final compounds used in the *in vitro* experiments were determined via ^{1}H NMR using an internal standard. All final compounds were lyophilized (Christ Alpha 2-4 LDplus) prior to usage to ensure dryness.

Synthetic Methods

All reagents were used as received unless otherwise noted. Solvents were purchased in the best quality available, anhydrous solvents were stored under nitrogen and dried over activated molecular sieves (4 Å, 1.6-2.6mm, Sigma-Aldrich). Reactions were monitored by thin layer chromatography (TLC) using SiliCycle TLC silica gel 60 F254 with UV light (254 nm) as a visualizing agent and acidic ceric ammonium molybdate (CAM) or potassium permanganate solutions and heat as developing agents. Purification was achieved by either: flash column chromatography with silica gel (230-400 mesh), a size-exclusion column with sephadex LH-20, or ion-exchange chromatography with a sodium charged Dowex 50WX8, 50-100 mesh resin. The Dowex resin was purchased in its protonated form and was converted to the sodium charged form by washing the resin with milli-Q H_2O until a neutral pH was achieved, charging with 1 M NaOH until a basic pH was achieved, and washing again with milli-Q H_2O until a neutral pH was achieved. No unexpected or unusually high safety hazards were encountered during this work.

Synthesis Schemes

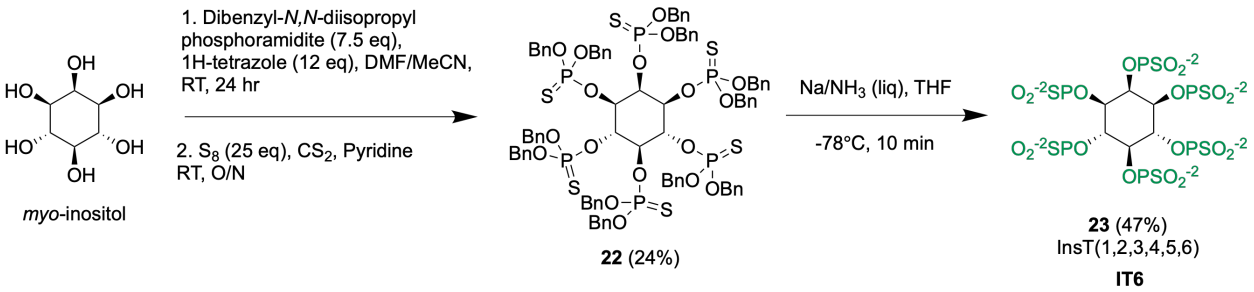

Figure 7. Scheme for the synthesis of hexakis-thiophosphate-*myo*-inositol (IT6). DMF, dimethylformamide; RT, room temperature; O/N, overnight; THF, tetrahydrofuran.

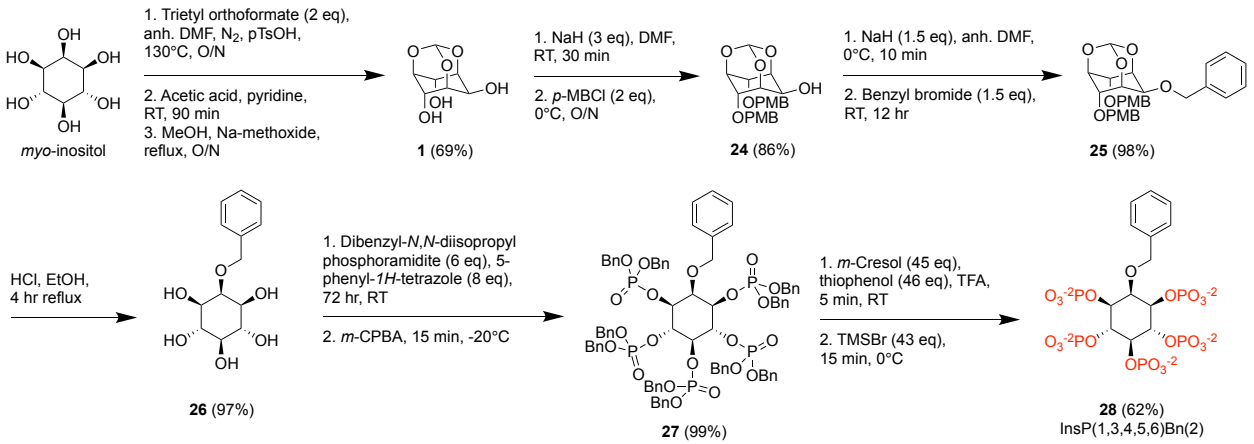

Figure 8. Scheme for the synthesis of 1,3,4,5,6-phosphate-2-*O*-benzyl-*myo*-inositol (IP5Bn). DMF, dimethylformamide; pTsOH, *p*-toluenesulfonic acid; RT, room temperature; O/N, overnight; *p*-MBCl, 4-methoxybenzyl chloride; *m*-CPBA, meta-chloroperoxybenzoic acid; TFA, trifluoroacetic acid; TMSBr, trimethylsilyl bromide.

Synthesis

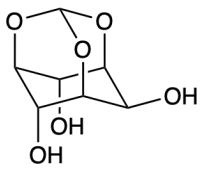

1,3,5-*O*-Methylidyne-*myo*-inositol (1)

Synthesis **of 1** was performed as described previously.[30] To a stirred suspension of dry *myo*-inositol (13.50 g, 75.00 mmol) in anhydrous DMF (90 mL) anhydrous triethyl orthoformate (22.40 mL, 135.00 mmol) and *p*-toluenesulfonic acid monohydrate (3.60 g, 18.90 mmol) were added under a nitrogen atmosphere. The reaction mixture was heated to 130°C overnight and was allowed to cool to room temperature before being concentrated *in vacuo*. Pyridine (40 mL) and acetic anhydride (40 mL) were added. The mixture was stirred at room temperature for 90

min and then put on ice overnight. A white precipitate formed which was filtered, washed with cyclohexane (3 x 30 mL), and dried. The white solid was taken up in dry methanol (100 mL) and sodium methoxide (0.88 g, 16.40 mmol) was added. The stirred mixture was heated to reflux overnight. The solution was allowed to cool to room temperature, quenched with DOWEX 50W X8 resin (H^+ form) until a neutral pH was reached, and filtered. It was dried over anhydrous $MgSO_4$, filtered, and concentrated *in vacuo* to afford compound **1** as a white solid (9.86 g, 51.85 mmol, 69% yield).

SMILES: O[C@H]([C@H](O1)[C@H]2O)[C@H]3O[C@@H]1O[C@@H]2[C@H]3O

^{1}H NMR (600 MHz, D_2O): δ 5.59 (d, J = 1.4 Hz, 1H, C_H), 4.57 (t, J = 4.0 Hz, 2H, H_4-H_6), 4.34-4.32 (m, 1H, H_2), 4.27-4.26 (m, 1H, H_5), 4.24-4.22 (m, 2H, H_1-H_3).

^{1}H NMR spectrum is in agreement with the literature report.[30]

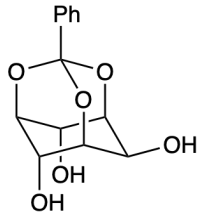

***myo*-Inositol-1,3,5-orthobenzoate (2)**

Synthesis of **2** was performed as described previously.[31] To a stirred suspension of dry *myo*-inositol (9.00 g, 50.00 mmol) and camphorsulfonic acid (232 mg, 1.00 mmol) in anhydrous DMSO (30 mL) trimethyl orthobenzoate (10 mL, 55.00 mmol) was added. The reaction mixture was heated to 80ºC under vacuum (260 mbar) for 6 hr on a rotary evaporator. The resulting solution was cooled to room temperature and the catalyst was neutralized by addition of triethylamine (1.00 mL). The reaction mixture was concentrated *in vacuo*. Hot ethyl acetate (500 mL) was added, and the mixture was then filtered through a pad of silica gel. The resulting filtrate was concentrated *in vacuo* and the homogenous solution was left in the refrigerator overnight. The precipitate was then filtered to afford compound **2** as a white filtrate (6.91 g, 26.00 mmol, 77% yield).

SMILES: O[C@H]([C@H](O1)[C@H]2O)[C@H]3O[C@]1(C4=CC=CC=C4)O[C@@H]2[C@H]3O

^{1}H NMR (600 MHz, DMSO-d_6): δ 7.56-7.55 (m, 2H, H_{Ph}), 7.38-7.32 (m, 3H, H_{Ph}), 5.53 (s, 2H, 2 × OH), 5.33 (d, J = 6.3 Hz, 1H, OH), 4.40 (t, J = 4.1 Hz, 2H, H_4 and H_6), 4.22-4.20 (dt, J = 3.7, 1.7 Hz, 1H, H_5), 4.16-4.15 (m, 2H, H_1 and H_3), 4.08 (br s, 1H, H_2).

^{1}H NMR spectrum is in agreement with the literature report.[31]

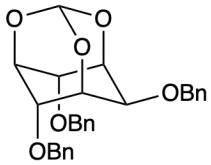

2,4,6-Tri-*O*-benzyl-*myo*-inositol-1,3,5-*O*-orthoformate (3)

Synthesis of **3** was performed as described previously.[32] To a stirred solution of compound **1** (2.52 g, 13.25 mmol) in anhydrous DMF (40 mL) NaH (60% dispersion in mineral oil, 1.34 g, 55.65 mmol) was added portionwise at 0°C, under a nitrogen atmosphere. The reaction mixture was stirred at 0°C for 30 min and then benzyl bromide (6.30 mL, 53.00 mmol) was added. The reaction mixture was left at room temperature for 24 hr. At this time, NaH (60% dispersion in mineral oil, 0.57 g, 23.85 mmol) was added because the reaction was incomplete. After 42 hr, the reaction mixture was carefully quenched with a few drops of H_2O and concentrated *in vacuo*. The residue was dissolved in DCM (200 mL), washed successively with H_2O (200 mL) and brine (200 mL), dried ($MgSO_4$), filtered, and concentrated *in vacuo* to give an oil as the crude product. Diethyl ether was added (20 mL) and the mixture was stirred vigorously. After a few minutes, the solid was filtered and washed successively with diethyl ether (30 mL) and methanol (30 mL) to afford compound **3** as a white solid (3.56 g, 7.45 mmol, 58% yield).

SMILES: [C@@H]1(O[C@@H]2O3)[C@H]([C@H](O2)[C@H](OCC4=CC=CC=C4)[C@H]3[C@H]1OCC5=CC=CC=C5)OCC6=CC=CC=C6

^{1}H NMR (600 MHz, $CDCl_3$): δ 7.40-7.21 (m, 15H, H_{Ph}), 5.55 (d, J = 0.5 Hz, 1H, C_H), 4.66 (s, 2H, CH_2), 4.56 (dd, J = 81.6, 11.6 Hz, 4H, 2 x CH_2), 4.45 (m, 1H, H_2), 4.35 (t, J = 3.5 Hz, 2H, H_1-H_3 or H_4-H_6), 4.31-4.30 (m, 2H, H_1-H_3 or H_4-H_6), 4.07 (d, J = 1.0 Hz, 1H, H_5).

^{1}H NMR spectrum is in agreement with the literature report.[32]

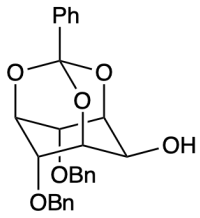

4,6-Di-*O*-benzyl-*myo*-inositol-1,3,5-orthobenzoate (4)

Synthesis of **4** was performed as described previously.[31] To a stirred solution of compound **2** (192 mg, 0.72 mmol) in anhydrous DMF (2.30 mL) NaH (60% dispersion in mineral oil, 66.40 mg, 1.66 mmol) was added portion-wise at 0°C, under a nitrogen atmosphere. The reaction mixture was stirred at 0°C for 30 min and then benzyl bromide (0.19 mL, 1.58 mmol) was added. The reaction mixture was allowed to warm to room temperature for 16 hr and then quenched with methanol dropwise (2 mL). H_2O (30 mL) and DCM (30 mL) were added. The aqueous layer was extracted with DCM (3 x 50 mL). Organic layers were recombined, washed with H_2O (30 mL), brine (30 mL), dried ($MgSO_4$), filtered, and concentrated *in vacuo*. Purification was achieved by flash chromatography on silica gel (cyclohexane/EtOAc 9/1 to 7/3) to afford compound **4** as a white solid (121 mg, 0.27 mmol, 38% yield).

SMILES: O[C@H]([C@H](O1)[C@H]2OCC3=CC=CC=C3)[C@H]4O[C@]1(C5=CC=CC=C5)O[C@@H]2[C@H]4OCC6=CC=CC=C6

^{1}H NMR (600 MHz, $CDCl_3$): δ 7.76-7.75 (m, 2H, H_{Ph}), 7.49-7.46 (m, 3H, H_{Ph}), 7.43-7.38 (m, 10H, H_{Ph} under $CDCl_3$), 4.76 (dd, J = 11.5 Hz, 4H, 2 × CH_2), 4.68 (sept, J = 1.8 Hz, 1H, H_5), 4.60 (t, J = 3.9 Hz, 2H, H_4 and H_6), 4.55 (m, J = 1.8 Hz, 2H, H_1 and H_3), 4.39 (d, J = 11.4 Hz, 1H, H_2), 3.27 (d, J = 11.7 Hz, 1H, OH).

^{1}H NMR spectrum is in agreement with the literature report.[31]

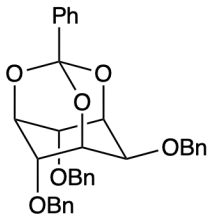

1,3,5-*O*-Orthobenzoate-2,4,6-tri-*O*-benzyl-*myo*-inositol (5)

Synthesis of **5** was performed as described previously.[33] To a stirred solution of compound **2** (4.00 g, 15.02 mmol) in dry DMF (7 mL), NaH (60% dispersion in mineral oil, 3.60 g, 90.12

mmol) was added portion-wise at 0°C, under a nitrogen atmosphere. The mixture was stirred at 0°C for 45 min and then benzyl bromide (10.70 mL, 90.00 mmol) was added. The reaction was allowed to warm to room temperature overnight and then slowly quenched with H_2O. The residue was dissolved in EtOAc (200 mL), washed successively with water (200 mL) and brine (200 mL), dried ($MgSO_4$), filtered, and concentrated *in vacuo*. Purification was achieved by flash chromatography on silica gel (cyclohexane/EtOAc 9/1) to afford compound **5** as a white solid (6.21 g, 11.57 mmol, 77% yield).

SMILES: [C@@H]1(O[C@]2(C3=CC=CC=C3)O4)[C@H]([C@H](O2)[C@H](OCC5=CC=CC=C5)[C@H]4[C@H]1OCC6=CC=CC=C6)OCC7=CC=CC=C7

^{1}H NMR (600 MHz, $CDCl_3$): δ 7.67-7.66 (m, 2H, H_{Ph}), 7.42-7.22 (m, 18H, H_{Ph}), 4.69 (s, 2H, CH_2), 4.65 (d, J = 11.6 Hz, 2H, CH_2), 4.58-4.56 (m, 1H, H_2), 4.53-4.51 (m, 4H, CH_2 and H_1-H_3 or H_4-H_6), 4.47 (t, J = 3.9 Hz, 2H, H_1-H_3 or H_4-H_6), 4.12 (t, J = 1.8 Hz, 1H, H_5).

^{1}H NMR spectrum is in agreement with the literature report.[33]

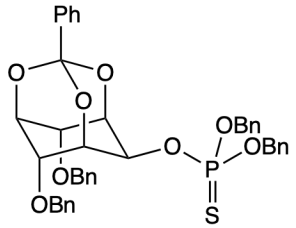

4,6-Di-*O*-benzyl-*myo*-inositol-1,3,5-orthobenzoate-2-*O,O*-dibenzylthiophosphate (6)

To a stirred solution of compound **4** (121 mg, 0.27 mmol) in anhydrous DCM (6 mL) was added, under a nitrogen atmosphere, 5-phenyl-1*H*-tetrazole (158 mg, 1.08 mmol) and dibenzyl-*N*,*N*-diisopropyl phosphoramidite (0.18 mL, 0.54 mmol) dropwise. The mixture was stirred at room temperature overnight. Thereafter, a solution of DMF and pyridine (3.30 mL, 1:1) were added followed by sulfur (52 mg, 1.62 mmol). The reaction was stirred at room temperature overnight, then quenched with H_2O (20 mL). The aqueous layer was extracted with EtOAc (3 x 50 mL). Organic layers were recombined, washed with brine (50 mL), dried ($MgSO_4$), filtered and concentrated *in vacuo*. Purification was achieved by flash chromatography on silica gel (cyclohexane/EtOAc, 9/1) to afford compound **6** as a yellowish gum (119 mg, 0.27 mmol, 61% yield).

SMILES: S=P(OCC1=CC=CC=C1)(OCC2=CC=CC=C2)O[C@H]([C@H](O3)[C@H]4O CC5=CC=CC=C5)[C@H]6O[C@]3(C7=CC=CC=C7)O[C@@H]4[C@H]6OCC8=CC=CC=C8

^{1}H NMR (600 MHz, $CDCl_3$): δ 7.62 (dd, J = 7.9, 1.8 Hz, 2H, H_{Ph}), 7.37-7.25 (m, 23H, H_{Ph}), 5.22 (dt, J = 10.1, 2.0 Hz, 1H, H_2), 5.17- 5.07 (m, 4H, 2 × P-OCH_2), 4.67-4.62 (m, 6H, 2 × C-OCH_2, H_1 and H_3), 4.57 (dq, J = 3.5, 1.8 Hz, 1H, H_5), 4.46 (t, J = 3.8 Hz, 2H, H_4 and H_6).

^{31}P NMR (203 MHz, $CDCl_3$): δ 67.0 (P-C_2).

^{13}C NMR (151 MHz, $CDCl_3$): δ 137.5 (2 × Cq_{Ph}), 137.1 (Cq_{Ph}), 135.8 (Cq_{Ph}), 135.7 (Cq_{Ph}), 129.6 (CH_{Ph}), 128.6 (CH_{Ph}), 128.5 (CH_{Ph}), 128.5 (CH_{Ph}), 128.1 (CH_{Ph}), 128.1 (CH_{Ph}), 128.0 (CH_{Ph}), 125.5 (CH_{Ph}), 107.9 (Cq_{Ph}), 73.8 (C_4 -C_6), 72.4 (d, J = 5.0 Hz, C_1-C_3), 71.7 (2 × $\underline{C}H_2$-OC), 70.0 (d, J = 5.5 Hz, 2 × CH_2-OP), 69.1 (C_5), 67.6 (d, $^{2}J_{C\text{-}P}$ = 4.4 H, C_2).

HRMS FTMS E^{+}. Calculated for $C_{41}H_{39}NaO_8PS$ $[M+Na]^{+}$ 745.1995; found 745.1973.

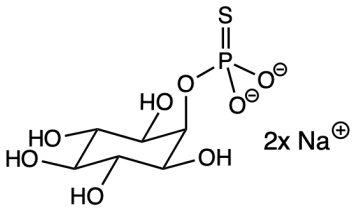

***myo*-Inositol-2-*O*-thiophosphate (7)**

To a stirred solution of compound **6** (105 mg, 0.16 mmol) in anhydrous THF (3 mL) liquid NH_3 (20 mL) was added under a nitrogen atmosphere at -78°C. Sodium was added in small pieces until the solution turned dark blue. The reaction was stirred for 10 min, then quenched with a saturated NH_4Cl solution. NH_3 was slowly evaporated overnight, and the remaining solution was extracted with DCM (10 mL). Purification of the aqueous layer by Sephadex LH-20 (100% H_2O) followed by cation exchange on DOWEX 50W X8 (Na^{+} form) and freeze-drying provided compound **7** as a yellowish lyophilizate (37 mg, 0.12 mmol, 76% yield).

SMILES: O[C@H]1[C@H](O)[C@@H](O)[C@H](O)[C@H](OP([O-2])([O])=S)[C@@H]1O

^{1}H NMR (600 MHz, D_2O): δ 4.73 (dt, J = 10.0, 2.7 Hz, 1H, H_2), 3.74 (t, J = 9.7 Hz, 2H, H_4 and H_6), 3.53 (dd, J = 9.9, 1.6 Hz, 2H, H_1 and H_3), 3.28 (t, J = 9.4 Hz, 1H, H_5).

^{31}P NMR (162 MHz, D_2O): δ 45.8 (P-C_2).

^{13}C NMR (151 MHz, D_2O): δ 76.0 (d, J = 6.6 Hz, C_2), 74.4 (C_5), 73.2 (C_4-C_6), 71.4 (d, J = 3.3 Hz, C_1-C_3).

HRMS FTMS E^{-}. Calculated for $C_6H_{12}O_8PS$ $[M-H]^-$ 274.9996; found 275.0000.

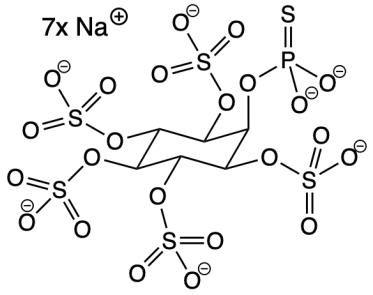

2-(*O*-Thiophosphate)-*myo*-inositol-1,3,4,5,6-penta-*O*-sulfate (8)

To a stirred suspension of compound **7** (11 mg, 0.034 mmol) in dry DMF (0.60 mL) a solution of TFA (10% in DMF) and sulphur trioxide *N*,*N*-dimethylformamide complex (221 mg, 1.44 mmol) was added. The solution was stirred at room temperature for 30 min then quenched with NaOH (1M) until pH 8. Methanol (3 mL) was added, and salts were filtered *in vacuo*. Purification of the precipitate by size exclusion chromatography (LH-20, 100% H_2O) followed by freeze drying provided compound **8** as a white lyophilizate (5.20 mg, 0.0062 mg, 19% yield).

SMILES: [O-2]P(O[C@H]1[C@@H](OS([O-])(=O)=O)[C@H](OS(=O)([O-])=O)[C@@H](OS(=O)([O-])=O)[C@H](OS(=O)([O-])=O)[C@H]1OS(=O)([O-])=O)([O])=S

^{1}H NMR (600 MHz, D_2O): δ 5.30 (s, 2H, H_2-H_5), 4.92 (s, 4H, H_1-H_3-H_4-H_6).

^{31}P NMR (162 MHz, D_2O): δ 77.98 (P-C_2).

^{13}C NMR (151 MHz, D_2O): δ 75.10 (d, J = 3.3 Hz), 74.07.

HRMS FTMS E^{-}. Calculated for $C_6H_6O_{23}Na_5PS_6$ $[M+5Na]^{2-}$ 391.8431; found 391.8427.

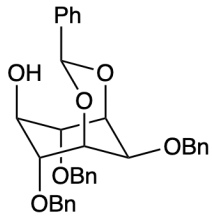

1,3-*O*-Phenylacetal-2,4,6-tri-*O*-benzyl-*myo*-inositol (9)

Synthesis of **9** was performed as described previously.[33] To a stirred solution of compound **5** (1.07 g, 2.00 mmol) in dry DCM (16 mL) a solution of DIBAL-H (4 mL, 1M in toluene) was added dropwise at 0°C under a nitrogen atmosphere. The reaction was allowed to warm to room

temperature over 2 hr and then poured into a stirred mixture of saturated Na/K tartrate (10 mL) and saturated NH_4Cl (10 mL) and stirred for 2 hr. The heterogenous solution was extracted with EtOAc (2 x 100 mL). Organic layers were recombined, washed with brine (100 mL), dried ($MgSO_4$), filtered, and evaporated *in vacuo*. Purification was achieved by flash chromatography on silica gel (cyclohexane/EtOAc, 8/2) to afford compound **9** as a clear oil (607 mg, 1.13 mmol, 57% yield).

SMILES: O[C@@H]1[C@H]([C@H](O[C@@H](C2=CC=CC=C2)O3)[C@H](OCC4=CC=CC=C4)[C@H]3[C@H]1OCC5=CC=CC=C5)OCC6=CC=CC=C6

^{1}H NMR (600 MHz, $CDCl_3$): δ 7.54 (d, J = 9.5 Hz, 2H, H_{Ph}), 7.37 (d, J = 91.0 Hz, 18H, H_{Ph}), 5.72 (s, 1H, CH), 4.73 (s, 2H, CH_2), 4.70 (dd, J = 84.1, 11.7 Hz, 4H, 2 × CH_2), 4.42 (d, J = 2.5 Hz, 2H, H_1-H_3 or H_4-H_6), 4.00 (d, J = 8.5 Hz, 2H, H_1-H_3 or H_4-H_6), 3.80 (td, J = 8.6, 2.9 Hz, 1H, H_5), 3.62 (t, J = 2.5 Hz, 1H, H_2), 2.49 (d, J = 2.8 Hz, 1H, OH).

^{1}H NMR spectrum is in agreement with the literature report.[33]

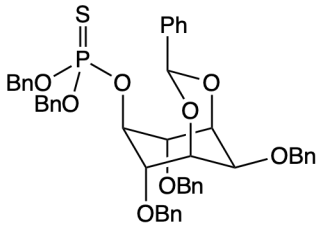

2,4,6-Tri-*O*-benzyl *myo*-inositol-1,3-orthobenzoate-5-*O,O*-dibenzylthiophosphate (10)

To a stirred solution of compound **9** (187 mg, 0.35 mmol) in anhydrous CH_2Cl_2 (8.5 mL) 5-phenyl-1*H*-tetrazole (205 mg, 1.40 mmol) and dibenzyl-*N*,*N*-diisopropyl phosphoramidite (0.23 mL, 0.69 mmol) were added dropwise under a nitrogen atmosphere. The mixture was stirred at room temperature overnight. Thereafter, a solution of DMF and pyridine (5.1 mL, 1:1) were added followed by sulfur (67 mg, 2.10 mmol). The reaction was stirred at room temperature overnight, then quenched with H_2O (20 mL). The aqueous layer was extracted with EtOAc (3 x 50 mL). Organic layers were recombined, washed with brine (50 mL), dried ($MgSO_4$), filtered, and concentrated *in vacuo*. Purification was achieved by flash chromatography on silica gel (cyclohexane/EtOAc, 9/1) to afford compound **10** as a yellow gum (206 mg, 0.25 mmol, 72% yield).

SMILES: S=P(OCC1=CC=CC=C1)(OCC2=CC=CC=C2)O[C@@H]3[C@H]([C@H](O[C@@H](C4=CC=CC=C4)O5)[C@H](OCC6=CC=CC=C6)[C@H]5[C@H]3OCC7=CC=CC=C7)OCC8=CC=CC=C8

^{1}H NMR (600 MHz, $CDCl_3$): δ 7.54-7.48 (m, 2H, H_{Ph}), 7.41-7.22 (m, 25H, H_{Ph}), 7.19-7.17 (m, 3H, H_{Ph}), 5.87 (s, 1H, CH), 5.04 – 4.91 (m, 4H, 2 × P-OCH_2), 4.88 (dt, J = 12.3, 6.1 Hz, 1H, H_5), 4.67 (s, 2H, C-OCH_2), 4.59 (dd, J = 26.2, 13.3 Hz, 4H, 2 × C-OCH_2), 4.36 (d, J = 2.4 Hz, 2H, H_1 and H_3), 4.14 (d, J = 6.1 Hz, 2H, H_4 and H_6), 3.70 (s, 1H, H_2).

^{31}P NMR (162 MHz, $CDCl_3$): δ 68.4 (P-C_5).

^{13}C NMR (151 MHz, $CDCl_3$): δ 138.2 (Cq_{Ph}), 138.0 (Cq_{Ph}), 137.4 (2 × Cq_{Ph}), 135.8 (Cq_{Ph}), 135.7 (Cq_{Ph}), 129.5 (CH_{Ph}), 128.6 (CH_{Ph}), 128.5 (CH_{Ph}), 128.5 (CH_{Ph}), 128.4 (CH_{Ph}), 128.0 (CH_{Ph}), 127.9 (CH_{Ph}), 127.8 (CH_{Ph}), 127.6 (CH_{Ph}), 126.7 (CH_{Ph}), 93.3 (CH-C_{Ph}), 81.2 (d, J = 4.4 Hz, C_4-C_6), 80.1 (d, $^{2}J_{C\text{-}P}$ = 6.6 Hz, C_5), 72.9 (C_1-C_3), 71.6 (2 × $\underline{C}H_2$-OC), 70.9 ($\underline{C}H_2$-OC), 69.9 (d, J = 4.4 Hz, 2 × CH_2-OP), 67.9 (C_2).

HRMS FTMS E^{+}. Calculated for $C_{48}H_{47}NaO_8PS$ $[M+Na]^+$ 837.2621; found 837.2653.

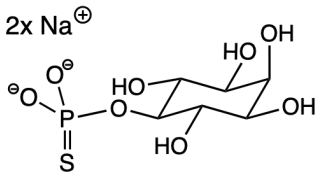

***myo*-Inositol-5-*O*-thiophosphate (11)**

To a stirred solution of compound **10** (206 mg, 0.25 mmol) in anhydrous THF (5.5 mL) liquid NH_3 (20 mL) was added at -78°C under a nitrogen atmosphere. Sodium was added in small pieces until the solution turned dark blue. The reaction was stirred for 10 min then quenched with a saturated NH_4Cl solution. NH_3 was slowly evaporated overnight, and the remaining solution was then extracted with DCM (20 mL). Purification of the aqueous layer by Sephadex LH-20 (100% H_2O) followed by cation exchange on DOWEX 50W X8 (Na^+ form) and freeze-drying provided compound **11** as a yellowish lyophilizate (34 mg, 0.11 mmol, 43% yield).

SMILES: O[C@H]1[C@H](OP([O-])([O-])=S)[C@@H](O)[C@H](O)[C@H](O)[C@@H]1O

^{1}H NMR (600 MHz, D_2O): δ 4.05 (t, J = 3.0 Hz, 1H, H_2), 4.00 (q, J = 9.3 Hz, 1H, H_5), 3.77 (t, J = 9.6 Hz, 2H, H_4 and H_6), 3.62 (dd, J = 10.1, 3.0 Hz, 2H, H_1 and H_3).

^{31}P NMR (162 MHz, D_2O): δ 45.5 (P-C_5).

^{13}C NMR (151 MHz, D_2O): δ 78.5 (d, J = 6.6 Hz, C_5), 72.0 (C_2), 71.9 (d, J = 3.3 Hz, C_4-C_6), 71.0 (C_1-C_3).

HRMS FTMS E$^-$. Calculated for $C_6H_{12}O_8PS$ $[M-H]^-$ 274.99960; found 274.99975.

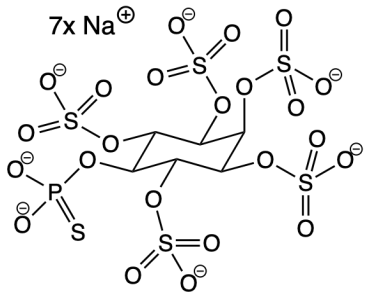

5-(*O*-Thiophosphate)-*myo*-inositol-1,2,3,4,6-penta-*O*-sulfate (12)

To a stirred suspension of compound **11** (20.1 mg, 0.063 mmol) in dry DMF (0.60 mL) a solution of TFA (10% in DMF) and sulphur trioxide *N*,*N*-dimethylformamide complex (405 mg, 2.65 mmol) were added. The solution was stirred at room temperature for 30 min then quenched with NaOH (1M) until pH 8. Methanol (3 mL) was added, and salts were filtered *in vacuo*. Purification of the precipitate by size exclusion chromatography (LH-20, 100% H_2O) followed by freeze drying provided compound **12** as a white lyophilizate (9.1 mg, 0.011 mmol, 17% yield).

SMILES: [O-]S(O[C@H]1[C@@H](OS([O-])(=O)=O)[C@H](OS(=O)([O-])=O)[C@@H](OP([O-])([O-])=S)[C@H](OS(=O)([O-])=O)[C@H]1OS(=O)([O])=O)(=O)=O

^{1}H NMR (600 MHz, D_2O): δ 5.05-4.87 (m, 5H), 4.54 (d, J = 15.9 Hz, 1H).

^{31}P NMR (162 MHz, D_2O): δ 77.98 (P-C_5).

^{13}C NMR (151 MHz, D_2O): δ 75.66, 73.74.

HRMS FTMS E$^-$. Calculated for $C_6H_7O_{23}Na_3PS_6$ $[M+3Na+H]^{3-}$ 246.23832; found 246.23833.

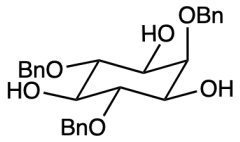

2,4,6-Tri-*O*-benzyl-*myo*-inositol (13)

Synthesis of **13** was performed as described previously.[32] To a stirred suspension of compound **3** (3.52 g, 7.64 mmol) in MeOH (60 mL) a solution of HCl (1 N, 8 mL) was added. The mixture

was heated to reflux for 3 hr and allowed to cool to room temperature before evaporation *in vacuo*. Purification was achieved by flash chromatography on silica gel (Hexane/EtOAc, 7/3 to 4/6) to afford compound **13** as a colorless oil (3.39 g, 7.52 mmol, 98% yield).

SMILES: O[C@H]1[C@H](OCC2=CC=CC=C2)[C@@H](O)[C@@H](OCC3=CC=CC=C3)[C@@H](O)[C@@H]1OCC4=CC=CC=C4

^{1}H NMR (600 MHz, $CDCl_3$): δ 7.40-7.30 (m, 15H, H_{Ph}), 4.87 (s, 4H, 2 x CH_2), 4.85 (s, 2H, CH_2), 4.01 (t, J = 2.7 Hz, 1H, H_2), 3.69-3.66 (m, 2H, H_4-H_6), 3.59-3.53 (m, 3H, H_5, H_1-H_3), 2.56 (br s, 1H, OH), 2.40 (d, J = 5.7 Hz, 2H, 2 x OH).

^{1}H NMR spectrum is in agreement with the literature report.[32]

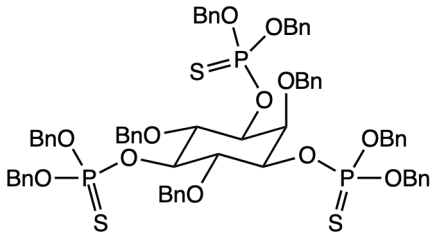

1,3,5-*O,O*-Dibenzylthiophosphate-2,4,6-tri-*O*-benzyl-*myo*-inositol (14)

To a stirred solution of compound **13** (300 mg, 0.67 mmol) in anhydrous DCM (10 mL) 5-phenyl-1*H*-tetrazole (1.17 g, 7.99 mmol) and dibenzyl-*N,N*-diisopropyl phosphoramidite (1.34 mL, 4.00 mmol) were added dropwise under a nitrogen atmosphere. The mixture was stirred at room temperature overnight. Thereafter, DMF and pyridine (5 mL, 1:1) were added followed by sulfur (342 mg, 10.70 mmol). The reaction was stirred at room temperature overnight, then quenched with H_2O (80 mL). The aqueous layer was extracted with DCM (3 x 100 mL). Organic layers were combined, washed with brine (100 mL), dried ($MgSO_4$), filtered, and concentrated *in vacuo*. Purification was achieved by flash chromatography on silica gel (Hexane/EtOAc, 9/1) to afford compound **14** as a white solid (375 mg, 0.29 mmol, 44% yield).

SMILES: S=P(OCC1=CC=CC=C1)(OCC2=CC=CC=C2)O[C@H]3[C@H](OCC4=CC=CC=C4)[C@@H](OP(OCC5=CC=CC=C5)(OCC6=CC=CC=C6)=S)[C@H](OCC7=CC=CC=C7)[C@@H](OP(OCC8=CC=CC=C8)(OCC9=CC=CC=C9)=S)[C@H]3OCC%10=CC=CC=C%10

^{1}H NMR (600 MHz, $CDCl_3$): δ 7.36-6.90 (m, 45H, H_{Ph}), 4.96-4.67 (m, 18H, CH_2, H_2, H_5), 4.56-4.53 (m, 2H, CH_2), 4.47 (td, J = 10.5, 2.5 Hz, 2H, H_1-H_3), 4.10 (t, J = 9.5 Hz, 2H, H_4-H_6).

^{31}P NMR (203 MHz, $CDCl_3$): δ 69.3 (P-C_5), 67.6 (P-C_1, P-C_3).

^{13}C NMR (125 MHz, $CDCl_3$): δ 138.7 (Cq_{Ph}), 138.4 (2 x Cq_{Ph}), 136.0 (Cq_{Ph}), 136.0 (Cq_{Ph}), 135.8 (Cq_{Ph}), 135.7 (Cq_{Ph}), 135.7 (Cq_{Ph}), 135.7 (Cq_{Ph}), 128.6 (CH_{Ph}), 128.6 (CH_{Ph}), 128.5 (CH_{Ph}), 128.4 (CH_{Ph}), 128.4 (CH_{Ph}), 128.3 (CH_{Ph}), 128.2 (CH_{Ph}), 128.1 (CH_{Ph}), 128.1 (CH_{Ph}), 127.8 (CH_{Ph}), 127.6 (CH_{Ph}), 127.5 (CH_{Ph}), 127.2 (CH_{Ph}), 127.1 (CH_{Ph}), 80.0 (C_5), 78.0 - 77.9 (m, C_4-C_6, C_1-C_3), 77.6 (C_2), 75.6 (CH_2), 74.1 (2 x CH_2), 70.2 (d, $^2J_{CP}$ = 5.0 Hz, 2 x CH_2-OP), 69.8 (d, $^2J_{CP}$ = 5.0 Hz, 2 x CH_2-OP), 69.7 (d, $^2J_{CP}$ = 4.4 Hz, 2 x CH_2-OP).

HRMS FTMS E$^+$. Calculated for $C_{69}H_{69}O_{12}NaP_3S_3$ $[M+Na]^+$ 1301,30562; found: 1301.30032.

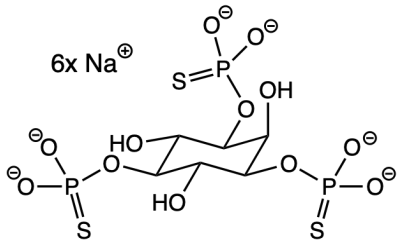

1,3,5-(Tri-*O*-thiophosphate)-*myo*-inositol (15)

To a stirred solution of compound **14** (140 mg, 109 µmol) in anhydrous THF (5 mL) liquid NH_3 (20 mL) was added at -78°C under a nitrogen atmosphere. Sodium was added in small pieces until the solution turned dark blue. The reaction was stirred for 10 min then quenched with a saturated NH_4Cl solution. NH_3 was slowly evaporated overnight, and the remaining solution was then extracted with DCM (20 mL). Purification of the aqueous layer by size exclusion chromatography (LH-20, 100% H_2O) followed by cation exchange on DOWEX 50W X8 (Na^+ form) and freeze-drying provided compound **15** as a white lyophilizate (51.2 mg, 85 µmol, 78% yield).

SMILES: O[C@H]1[C@H](OP([O-])([O-])=S)[C@@H](O)[C@H](OP([O-])([O-])=S)[C@H](O)[C@@H]1OP([O-])([O-])=S

^{1}H NMR (600 MHz, D_2O): δ 4.74 (t, J = 3.0 Hz, 1H, H_2), 4.21 (td, J = 9.6, 2.6 Hz, 2H, H_1-H_3), 4.13 (q, J = 9.6 Hz, 1H, H_5), 3.91 (t, J = 9.5 Hz, 2H, H_4-H_6).

^{31}P NMR (203 MHz, D_2O): δ 45.2 (P-C_5), 43.1 (P-C_1, P-C_3).

^{13}C NMR (151 MHz, D_2O): δ 78.8 (d, $^2J_{CP}$ = 7.0 Hz, C_5), 74.3 (d, $^2J_{CP}$ = 6.0 Hz, C_1-C_3), 71.5 (dd, J = 6.0, 3.3 Hz, C_4-C_6), 70.1 (C_2).

HRMS FTMS E$^-$. Calculated for $C_6H_{12}O_{12}Na_2P_3S_3$ $[M+2Na+3H]^-$ 510.85046; found: 510.85050.

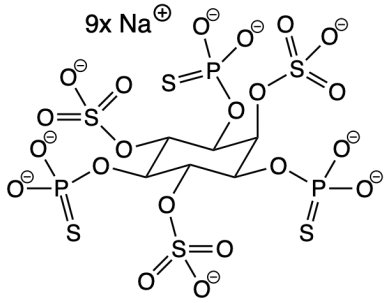

1,3,5-(Tri-*O*-thiophosphate)-*myo*-inositol-2,4,6-tri-*O*-sulfate (16)

To a stirred suspension of compound **15** (15.5 mg, 25.8 µmol) in dry DMF (0.50 mL) a solution of TFA (10% in DMF) and sulphur trioxide *N*,*N*-dimethylformamide complex (100 mg, 0.65 mmol) were added. The solution was stirred at room temperature for 30 min then quenched with NaOH (1M) until pH 8. Methanol (3 mL) was added, and salts were filtered *in vacuo*. Purification of the precipitate by size exclusion chromatography (LH-20, 100% H_2O) followed by freeze drying provided compound **16** as a white lyophilizate (11.7 mg, 12.9 µmol, 54% yield).

SMILES: [O-]P(O[C@H]1[C@H](OS(=O)([O-])=O)[C@@H](OP([O-])([O-])=S)[C@H](OS(=O)([O-])=O)[C@@H](OP([O-])([O-])=S)[C@H]1OS(=O)([O-])=O)([O-])=S

^{1}H NMR (600 MHz, D_2O): δ 5.22 (br s, 2H, H_4-H_6), 4.88 (d, J = 13.0 Hz, 2H, H_1-H_3), 4.79-4.74 (buried, m, 2H, H_5, H_2).

^{31}P NMR (203 MHz, D_2O): δ 44.9 (P-C_5, P-C_3, P-C_1).

^{13}C NMR (151 MHz, D_2O): δ 76.9 (C_4-C_6), 71.1 (d, $^2J_{CP}$ = 5.5 Hz, C_1-C_3), 70.3 (C_2), 68.5 (d, $^2J_{CP}$ = 5.0 Hz, C_5).

HRMS FTMS E$^-$. Calculated for $C_6H_{12}O_{21}P_3S_6$ $[M+6H]^{3-}$ 234.91415; found: 234.91431.

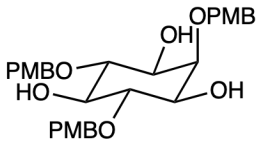

2,4,6-Tri-*O*-(*p*-methoxybenzyl)-*myo*-inositol (17)

Synthesis of **16** was performed as described previously.[48] To a stirred solution of compound **1** (2.00 g, 10.52 mmol) in dry DMF (15 mL) NaH (60% dispersion in mineral oil, 2.94 g, 73.64 mmol) was added portion-wise at 0°C. The suspension was stirred at 0°C for 30 min, then 4-methoxybenzyl chloride (6.15 mL, 42.08 mmol) was added and the mixture was allowed to warm to room temperature for 20 hr. The reaction was quenched with a slow addition of H_2O (100 mL) and extracted with DCM (3 x 150 mL). The organic layers were combined, washed with brine (200 mL), dried ($MgSO_4$), filtered, and evaporated *in vacuo*. The crude product was used in the next step without further purification.

MeOH (500 mL) and HCl (1 N, 50 mL) were added, and the suspension was stirred at room temperature for 5 days then neutralized with NaOH solution (1 M) until pH 7. Methanol was evaporated and H_2O (150 mL) was added. The aqueous layer was extracted with EtOAc (3 x 150 mL). The organic layers were combined, washed with brine (200 mL), filtered, and concentrated *in vacuo*. Purification was achieved by flash chromatography on silica gel (Hexane/EtOAc, 3/7) to afford compound **17** as a white solid (3.62 g, 6.69 mmol, 64% yield over two steps).

SMILES: O[C@H]1[C@H](OCC2=CC=C(OC)C=C2)[C@@H](O)[C@@H](OCC3=CC=C(OC)C=C3)[C@@H](O)[C@@H]1OCC4=CC=C(OC)C=C4

^{1}H NMR (600 MHz, $CDCl_3$): δ 7.31-7.25 (m, 6H, H_{Ph}), 6.92-6.89 (m, 6H, H_{Ph}), 4.78 (s, 4H, 2 x CH_2), 4.75 (s, 2H, CH_2), 3.98 (t, J = 2.8 Hz, 1H, H_2), 3.83 (s, 3H, OCH_3), 3.81 (s, 6H, 2 x OCH_3), 3.63-3.60 (m, 2H, H_4-H_6), 3.55-3.52 (m, 2H, H_1-H_3), 3.49 (td, J = 9.2, 2.1 Hz, 1H, H_5), 2.46 (d, J = 2.0 Hz, 1H, OH), 2.32 (d, J = 6.1 Hz, 2H, 2 x OH).

^{1}H NMR spectrum is in agreement with the literature report.[48]

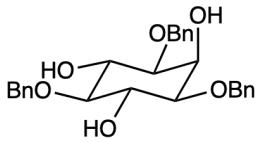

1,3,5-Tri-*O*-benzyl-*myo*-inositol (18)

Synthesis of **18** was performed as described previously.[49] To a stirred solution of compound **17** (3.61 g, 6.69 mmol) in dry DMF (20 mL) NaH (60% dispersion in mineral oil, 1.87 g, 46.76 mmol) was added portion-wise at 0°C. The suspension was stirred at 0°C for 30 min, then benzyl bromide (3.18 mL, 26.72 mmol) was added, and the mixture was allowed to warm to room

temperature for 4 days. The reaction was quenched with a slow addition of H_2O (100 mL) and extracted with DCM (3 x 150 mL). The organic layers were combined, washed with brine (200 mL), dried ($MgSO_4$) and evaporated *in vacuo*. The crude product was used in the next step without further purification. DCM (100 mL) was added, followed by a mixture of TFA and water (50 mL, 4:1) at room temperature. The mixture was stirred for 3 hr then evaporated *in vacuo*. DCM (100 mL) was added (150 mL). The organic layer was washed with $NaHCO_3$ saturated solution (100 mL), brine (100 mL), dried (Na_2SO_4), filtered and concentrated *in vacuo*. The resulting oil was purified via flash column chromatography on silica gel (cyclohexane/ethyl acetate, 80/20 to 70/30) to afford the product as a white solid (170 mg, 69% yield). Purification was achieved by flash chromatography on silica gel (Hexane/EtOAc, 8/2 to 5/5) to afford compound **18** as a yellowish solid (1.08 g, 2.40 mmol, 36% yield over two steps).

SMILES: O[C@H]1[C@H](OCC2=CC=CC=C2)[C@@H](O)[C@H](OCC3=CC=CC=C3)[C@H](O)[C@@H]1OCC4=CC=CC=C4

^{1}H NMR (600 MHz, $CDCl_3$): δ 7.35-7.22 (m, 15H, H_{Ph}), 4.84 (s, 2H, CH_2), 4.70-4.62 (m, 4H, 2 x CH_2), 4.20 (t, J = 2.8 Hz, 1H, H_2), 4.01 (td, J = 9.5, 1.9 Hz, 2H, H_4-H_6), 3.22-3.19 (m, 3H, H_1-H_3, H_5), 2.48 (d, J = 2.0 Hz, 2H, 2 x OH), 2.35 (br s, 1H, OH).

^{1}H NMR spectrum is in agreement with the literature report.[49]

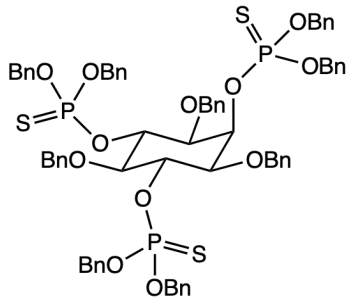

2,4,6-*O,O*-Dibenzylthiophosphate-1,3,5-tri-*O*-benzyl-*myo*-inositol (19)

To a stirred solution of compound **18** (300 mg, 0.67 mmol) in anhydrous DCM (10 mL) 5-phenyl-1*H*-tetrazole (1.17 g, 7.99 mmol) and dibenzyl-*N,N*-diisopropylphosphoramidite (1.34 mL, 4.00 mmol) were added dropwise under a nitrogen atmosphere. The mixture was stirred at room temperature for 48 hr. Thereafter, a solution of DMF and pyridine (5 mL, 1:1) was added followed by sulfur (342 mg, 10.65 mmol). The reaction was stirred at room temperature

overnight, then quenched with H_2O (80 mL). The aqueous layer was extracted with DCM (3 x 100 mL). Organic layers were combined, washed with brine (100 mL), dried ($MgSO_4$), filtered, and concentrated *in vacuo.* Purification was achieved by flash chromatography on silica gel (cyclohexane/EtOAc, 9/1) to afford compound **19** as a white solid (549 mg, 0.43 mmol, 64% yield).

SMILES: S=P(OCC1=CC=CC=C1)(OCC2=CC=CC=C2)O[C@H]3[C@@H](OCC4=CC=CC=C4)[C@H](OP(OCC5=CC=CC=C5)(OCC6=CC=CC=C6)=S)[C@@H](OCC7=CC=CC=C7)[C@H](OP(OCC8=CC=CC=C8)(OCC9=CC=CC=C9)=S)[C@H]3OCC%10=CC=CC=C%10

^{1}H NMR (600 MHz, $CDCl_3$): δ 7.47-6.90 (m, 45H, H_{Ph}), 5.66 (dt, J = 13.1, 2.4 Hz, 1H, H_2), 5.33-5.19 (m, 6H, CH_2, H_4-H_6), 4.98 (d, J = 11.1 Hz, 2H, CH_2), 4.94 (s, 2H, CH_2), 4.88 (t, J = 8.5 Hz, 2H, CH_2), 4.85 (t, J = 8.6 Hz, 2H, CH_2), 4.69-4.64 (m, 2H, CH_2), 4.58 (d, J = 11.1 Hz, 2H, CH_2), 4.47 (t, J = 11.5 Hz, 2H, CH_2), 3.71 (t, J = 9.5 Hz, 1H, H_5), 3.55 (dt, J = 9.9, 2.3 Hz, 2H, H_1-H_3).

^{31}P NMR (203 MHz, $CDCl_3$): δ 70.2 (P-C_4, P-C_6), 66.8 (P-C_2).

^{13}C NMR (125 MHz, $CDCl_3$): δ 138.5 (Cq_{Ph}), 136.8 (2 x Cq_{Ph}), 136.2 (Cq_{Ph}), 136.2 (Cq_{Ph}), 136.1 (Cq_{Ph}), 136.1 (Cq_{Ph}), 136.0 (Cq_{Ph}), 136.0 (Cq_{Ph}), 128.4 (CH_{Ph}), 128.4 (CH_{Ph}), 128.4 (CH_{Ph}), 128.3 (CH_{Ph}), 128.2 (CH_{Ph}), 128.1 (CH_{Ph}), 128.1 (CH_{Ph}), 128.0 (CH_{Ph}), 127.9 (CH_{Ph}), 127.8 (CH_{Ph}), 127.8 (CH_{Ph}), 126.7 (CH_{Ph}), 80.0 (C_5), 79.2 (d, $^2J_{CP}$ = 6.0 Hz, C_4-C_6), 76.5 (C_1-C_3), 73.8 (CH_2), 72.9 (d, $^2J_{CP}$ = 6.0 Hz, C_2), 72.4 (2 x CH_2), 70.0 (d, $^2J_{CP}$ = 6.4 Hz, 2 x CH_2-OP), 69.8 (d, $^2J_{CP}$ = 4.1 Hz, 2 x CH_2-OP), 69.6 (d, $^2J_{CP}$ = 4.6 Hz, 2 x CH_2-OP).

HRMS FTMS E$^+$. Calculated for $C_{69}H_{69}O_{12}NaP_3S_3$ $[M+Na]^+$ 1301,30562; found: 1301.30491.

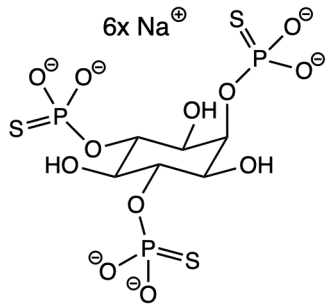

2,4,6-(Tri-*O*-thiophosphate)-*myo*-inositol (20)

To a stirred solution of compound **19** (204 mg, 0.16 mmol) in anhydrous THF (5 mL) liquid NH_3 (20 mL) was added at -78°C under an argon atmosphere. Sodium was added in small pieces until the solution turned dark blue. The reaction was stirred for 10 min at -78°C then quenched with a saturated NH_4Cl solution. NH_3 was slowly evaporated overnight, and the remaining solution was extracted with DCM (20 mL). The aqueous layer was purified by size exclusion chromatography (LH-20, 100% H_2O) followed by cation exchange on DOWEX 50W X8 (Na^+ form) and freeze-drying provided compound **20** as a yellowish lyophilizate (58.0 mg, 0.10 mmol, 61% yield).

SMILES: O[C@H]1[C@H](OP([O-])([O-])=S)[C@@H](O)[C@@H](OP([O-])([O-])=S)[C@@H](O)[C@@H]1OP([O-])([O-])=S

^{1}H NMR (600 MHz, D_2O): δ 4.75 (br s, 1H, H_2), 4.45 (q, J = 9.5 Hz, 2H, H_4-H_6), 3.70 (d, J = 9.7 Hz, 2H, H_1-H_3), 3.63 (t, J = 8.9 Hz, 1H, H_5).

^{31}P NMR (203 MHz, D_2O): δ 45.9 (P-C_2), 45.1 (P-C_4, P-C_6).

^{13}C NMR (151 MHz, D_2O): δ 77.6 (d, $^2J_{CP}$ = 7.2 Hz, C_4-C_6), 75.8 (d, $^2J_{CP}$ = 6.6 Hz, C_2), 74.3 (C_5), 71.1 (t, $^2J_{CP}$ = 3.3 Hz, C_1-C_3)

HRMS FTMS E$^-$. Calculated for $C_6H_{14}O_{12}P_3S_3$ $[M+5H]^-$ 466.88657; found: 466.88763.

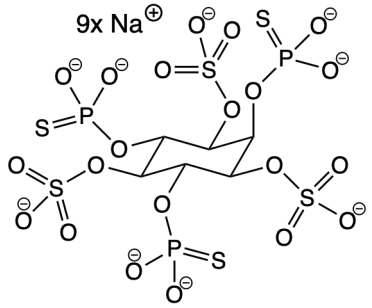

2,4,6-(Tri-*O*-thiophosphate)-*myo*-inositol-1,3,5-tri-*O*-sulfate (21)

To a stirred suspension of compound **20** (17.8 mg, 29.70 µmol) in dry DMF (0.60 mL) a solution of TFA (10% in DMF) and sulphur trioxide *N*,*N*-dimethylformamide complex (114 mg, 0.74 mmol) was added. The solution was stirred at room temperature for 30 min then quenched with NaOH (1M) until pH 8. MeOH (5 mL) was added, and salts were filtered *in vacuo*. Purification of the precipitate by size exclusion chromatography (LH-20, 100% H_2O) followed by freeze drying provided compound **21** as a white lyophilizate (17.5 mg, 20.8 µmol, 70% yield).

SMILES: [O-]P(O[C@H]1[C@@H](OS(=O)([O-])=O)[C@H](OP([O-])([O-])=S)[C@@H](OS(=O)([O-])=O)[C@H](OP([O-])([O-])=S)[C@H]1OS(=O)([O-])=O)([O-])=S

^{1}H NMR (600 MHz, D_2O): δ 5.15 (d, J = 14.3 Hz, 2H, H_4-H_6), 5.02-4.99 (m, 2H, H_1-H_3), 4.89 (dt, J = 14.8, 3.9 Hz, 1H, H_2), 4.83 (br s, 1H, H_5).

^{31}P NMR (203 MHz, D_2O): δ 44.7 (P-C_4, P-C_6), 44.2 (P-C_2).

^{13}C NMR (151 MHz, D_2O): δ 77.3 (C_1-C_3), 74.2 (C_5), 71.1 (d, $^{2}J_{CP}$ = 4.4 Hz, C_4-C_6), 64.8 (d, $^{2}J_{CP}$ = 4.4 Hz, C_2).

HRMS FTMS E$^-$. Calculated for $C_6H_{12}O_{21}P_3S_6$ $[M+6H]^{3-}$ 234.91415; found: 234.91420.

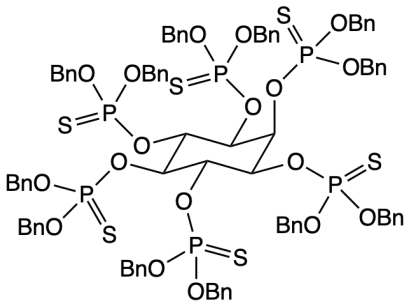

Hexakis-*O*,*O*-dibenzylthiophosphate-*myo*-inositol (22)

Synthesis of **22** was performed as described previously.[35] To a stirred suspension of *myo*-inositol (97 mg, 0.54 mmol) in an anhydrous mixture of DMF (14 mL) and acetonitrile (4 mL) 1*H*-tetrazole (14 mL, 0.45 M in acetonitrile) and dibenzyl-*N*,*N*-diisopropyl phosphoramidite (1.34 mL, 3.98 mmol) were added under a nitrogen atmosphere. The mixture was stirred at room temperature for 24 hr. Thereafter, pyridine (0.40 mL) and carbon disulfide (0.40 mL, 6.84 mmol) were added, followed by sulfur (427 mg, 13.34 mmol). The reaction was stirred at room temperature overnight then diluted with ethyl acetate (150 ml), washed with $NaHCO_3$ saturated solution (100 mL), brine (100 mL), dried ($MgSO_4$), filtered, and concentrated *in vacuo*. Purification was achieved by flash chromatography on silica gel (cyclohexane/ EtOAc 9/1 to 8/2) to afford compound **22** as a clear oil (236 mg, 0.13 mmol, 24% yield).

SMILES: S=P(OCC1=CC=CC=C1)(OCC2=CC=CC=C2)O[C@H]3[C@@H](OP(OCC4=CC=CC=C4)(OCC5=CC=CC=C5)=S)[C@H](OP(OCC6=CC=CC=C6)(OCC7=CC=CC=C7)=S)[C@@H](OP(OCC8=CC=CC=C8)(OCC9=CC=CC=C9)=S)[C@H](OP(OCC%10=CC=CC=C

%10)(OCC%11=CC=CC=C%11)=S)[C@H]3OP(OCC%12=CC=CC=C%12)(OCC%13=CC=CC=C%13)=S

^{1}H NMR (600 MHz, $CDCl_3$): δ 7.39-7.06 (m, 60H, H_{Ph}), 5.61-5.55 (m, 3H, H_2 or H_5 and H_1-H_3 or H_4-H_6), 5.49-5.46 (m, 2H, H_1-H_3 or H_4-H_6), 5.34 (d, J = 15.8 Hz, 1H, H_2 or H_5), 5.19-5.00 (m, 24H, CH_2).

^{31}P NMR (203 MHz, $CDCl_3$): δ 69.3, 68.8 (2 x P), 68.0.

^{13}C NMR (125 MHz, $CDCl_3$): δ 135.7 (Cq_{Ph}), 135.7 (Cq_{Ph}), 135.6 (Cq_{Ph}), 135.5 (Cq_{Ph}), 135.5 (Cq_{Ph}), 135.5 (Cq_{Ph}), 135.5 (Cq_{Ph}), 135.5 (Cq_{Ph}), 135.4 (Cq_{Ph}), 128.5 (CH_{Ph}), 128.5 (CH_{Ph}), 128.4 (CH_{Ph}), 128.4 (CH_{Ph}), 128.4 (CH_{Ph}), 128.3 (CH_{Ph}), 128.3 (CH_{Ph}), 128.3 (CH_{Ph}), 128.2 (CH_{Ph}), 128.2 (CH_{Ph}), 128.1 (CH_{Ph}), 128.0 (CH_{Ph}), 74.6 (C_1-C_3 or C_4-C_6), 74.0 (q, J = 4.7 Hz, C_1-C_3 or C_4-C_6), 70.5-70.4 (m, CH_2, C_2 and C_5), 70.3 (d, J = 5.0 Hz, CH_2), 70.2 (d, J = 4.4 Hz, CH_2), 70.2 (d, J = 5.5 Hz, CH_2).

HRMS FTMS E$^+$. Calculated for $C_{90}H_{90}O_{18}NaP_6S_6$ $[M+Na]^+$ 1859,2769; found: 1859,2687.

^{1}H NMR, ^{31}P NMR, and ^{13}C NMR spectrum is in agreement with the literature report.[35]

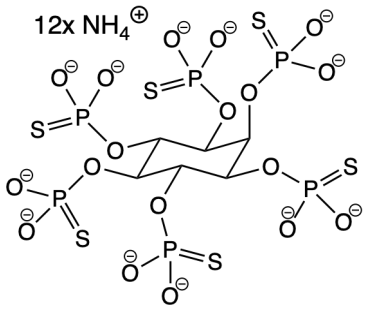

Hexakis-thiophosphate-*myo*-inositol (23)

Synthesis was performed as described previously.[35] To a stirred solution of compound **22** (235 mg, 0.13 mmol) in anhydrous THF (4 mL) liquid NH_3 (20 mL) was added at -78°C under a nitrogen atmosphere. Sodium was added in small pieces until the solution turned dark blue. The reaction was stirred for 10 min then quenched with a saturated NH_4Cl solution. NH_3 was slowly evaporated overnight, and the remaining solution was extracted with CH_2Cl_2 (10 mL). Purification of the aqueous layer was achieved by Sephadex LH-20 (100% H_2O) and freeze-drying provided the ammonium form of compound **23** as a white lyophilizate (57 mg, 59 µmol, 47% yield).

SMILES: [O-]P(O[C@H]1[C@@H](OP([O-])([O-])=S)[C@H](OP([O-])([O-])=S)[C@@H](OP([O-])([O-])=S)[C@H](OP([O-])([O-])=S)[C@H]1OP([O-])([O-])=S)([O-])=S

^{1}H NMR (600 MHz, D_2O): δ 4.87 (d, J = 13.4 Hz, 2H, H_1-H_3 or H_4-H_6), 4.83 (d, J = 11.8 Hz, 2H, H_1-H_3 or H_4-H_6), 4.72 (d, J = 14.5 Hz, 1H, H_2 or H_5), 4.55 (d, J = 14.1 Hz, 1H, H_2 or H_5).

^{31}P NMR (203 MHz, D_2O): δ 44.5 (P-C_2 or P-C_5), 43.1 (P-C_1, P-C_3 or P-C_4, P-C_6), 43.0 (P-C_1, P-C_3 or P-C_4, P-C_6), 42.9 (P-C_2 or P-C_5).

^{13}C NMR (151 MHz, D_2O): δ 74.4 (C_1-C_3 or C_4-C_6), 73.9-73.6 (C_1-C_3 or C_4-C_6), 71.1 (C_2 or C_5), 66.5 (C_2 or C_5).

HRMS FTMS E$^+$. Calculated for $C_6H_6Na_8O_{18}P_6S_6$ $[M+8Na]^{2-}$ 463.7748; found: 463.7733.

^{1}H NMR, ^{31}P NMR, and ^{13}C NMR spectrum is in agreement with the literature report.[35]

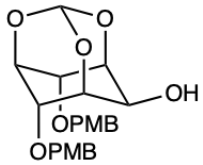

4,6-Bis-*O*-(4-methoxybenzyl)-*myo*-inositol monoorthoformate (24)

Synthesis was performed as described previously.[30] Compound **1** (300 mg, 1.58 mmol, 1 eq) was co-evaporated in toluene thrice. The quenched reactant was then dissolved in 4 mL of anhydrous DMF. NaH (60% dispersion in mineral oil, 95 mg, 3.96 mmol, 2.5 eq) was dissolved in 2 mL of anhydrous DMF, and the mixture was left to stir at room temperature for a few minutes. Compound **1** was then added dropwise to the reaction mixture. This was allowed to react for 30 min at room temperature. The reaction mixture was then cooled to 0°C. *para*-methoxy benzyl chloride (496 mg, 3.17 mmol, 2 eq) was added dropwise to the reaction mixture, and the solution was left to stir for 36 hr at 0°C. The reaction mixture was quenched with equal parts of methanol, concentrated, and separated between DCM and H_2O thrice. The organic layer was dried with $MgSO_4$, vacuum filtered, and concentrated. The crude product was purified via flash column chromatography (silica gel, gradient of 30, 35, 40, and 45% ethyl acetate/cyclohexane). The product was detected with 30% ethyl acetate/cyclohexane (R_f-value = 0.26) using UV light and a CAM stain. Compound **24** appeared as small white crystals (543 mg, 1.34 mmol, 86% yield).

SMILES: O[C@H]([C@H](O1)[C@H]2OCC3=CC=C(OC)C=C3)[C@H]4O[C@@H]1O[C@@H]2[C@H]4OCC5=CC=C(OC)C=C5

^{1}H-NMR (400 MHz, $CDCl_3$): δ 7.18 (d, J = 8.8 Hz, 4H, H_{oPh}), 6.82 (d, J = 8.4 Hz, 4H, H_{mPh}), 5.45 (s, 1H, H_7), 4.58 (d, J = 11.12, 2H, CH_2), 4.50 (d, J = 11.08, 2H, CH_2), 4.42-4.38 (m, 1H, H_5), 4.34 (t, J = 3.64, 2H, H_4-H_6), 4.20-4.18 (m, 2H, H_1-H_3), 4.16-4.13 (m, 1H, H_2), 3.80 (s, 6H, CH_3).

^{1}H NMR spectrum is in agreement with the literature report.[30]

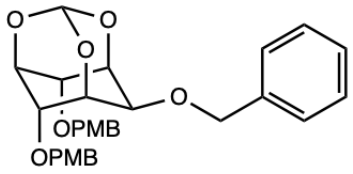

2-*O*-Benzyl-4,6-bis-*O*-(4-methoxybenzyl)-*myo*-inositol monoorthoformate (25)

Synthesis of **25** was performed as described previously.[50] Compound **24** (305 mg, 0.708 mmol, 1 eq) was combined with NaH (60% dispersion in mineral oil, 51 mg, 2.124 mmol, 3 eq) and 2 mL of anhydrous DMF and was stirred for 10 min at 0°C. The reaction mixture was warmed to room temperature and benzyl bromide (182 mg, 1.062 mmol, 1.5 eq) was added dropwise. The mixture was stirred for 48 hr at room temperature. The reaction mixture was quenched with methanol, concentrated, and separated between H_2O and DCM thrice. The organic layer was dried with Na_2SO_4, filtered, and concentrated. The crude product was purified via flash column chromatography (silica gel, 30% ethyl acetate/cyclohexane). The product was visible by UV light ad a CAM stain (R_f-value = 0.73; 30% ethyl acetate/cyclohexane). Compound **25** appeared as a clear viscous oil (238 mg, 0.458 mmol, 98% yield).

SMILES: COC(C=C1)=CC=C1CO[C@@H]2[C@@H]3[C@@H](OCC4=CC=CC=C4)[C@@H](O5)[C@H](OCC6=CC=C(OC)C=C6)[C@H]2O[C@@H]5O3

^{1}H-NMR (400 MHz, $CDCl_3$): δ 7.40-7.28 (m, 5H, H_{Bn}), 7.12 (d, J = 8.65 Hz, 4H, H_{oPh}), 6.81 (d, J = 8.67 Hz, 4H, H_{mPh}), 5.52 (d, J = 1.14 Hz, 1H, H_7), 4.64 (s, 2H, CH_2-Bn), 4.53 (d, J = 11.18 Hz, 2H, CH_2-PMB), 4.40 (d, J = 11.25 Hz, 2H, CH_2-PMB), 4.37 (sept, J = 1.68 Hz, 1H, H_5), 4.30 (t, J = 3.72 Hz, 2H, H_4-H_6), 4.27-4.23 (m, 2H, H_1-H_3), 4.01 (q, J = 1.48 Hz, 1H, H_2), 3.80 (s, 6H, CH_3).

^{1}H NMR spectrum is in agreement with the literature report.[50]

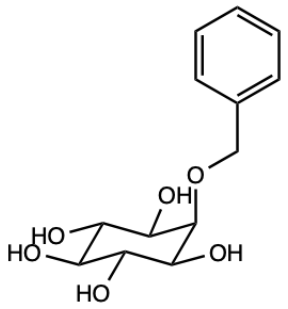

2-*O*-Benzyl-*myo*-inositol (26)

Synthesis of **26** was performed as described previously.[50] Compound **25** (187 mg, 0.359 mmol, 1 eq) was combined with 3 mL of ethanol and 1.5 mL of 1N HCl_{aq} at 90°C for 4 hr. The reaction mixture was concentrated, and the product was partitioned between H_2O and ethyl acetate thrice. The aqueous layer was concentrated, producing a white solid, compound **26** (94 mg, 0.348 mmol, 97% yield).

SMILES: O[C@H]1[C@H](O)[C@@H](O)[C@H](O)[C@@H](O)[C@H]1OCC2=CC=CC=C2

^{1}H-NMR (500 MHz, D_2O): δ 7.47 (d, J = 6.93 Hz, 2H, H_{Bn}), 7.42 (t, J = 7.34 Hz, 2H, H_{Bn}), 7.37 (t, J = 7.05 Hz, 1H, H_{Bn}), 4.83 (s, 2H, H_7), 4.02 (t, J = 2.61 Hz, 1H, H_2), 3.65 (t, J = 9.59 Hz, 2H, H_4-H_6), 3.58 (dt, J = 2.6, 10.1 Hz, 2H, H_1-H_3), 3.24 (t, J = 9.12 Hz, 1H, H_5).

^{1}H NMR spectrum is in agreement with the literature report.[50]

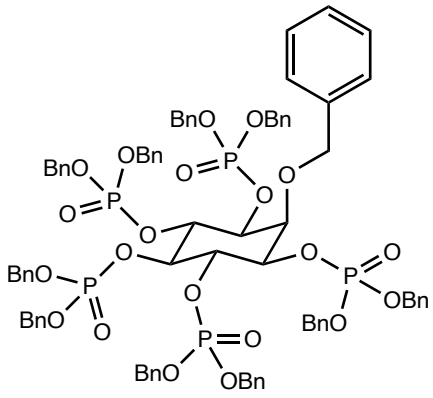

1,3,4,5,6-Penta-*O*-(dibenzyl-*N*,*N*-diisopropyl phosphoramidite)-2-*O*-benzyl-*myo*-inositol (27)

Synthesis of **27** was performed as described previously.[50] Compound **26** (202 mg, 0.746 mmol, 1 eq) was dried with toluene twice. Compound **26** was then combined with 1 mL of anhydrous

DCM, 5-phenyl-1*H*-tetrazole (335 mg, 2.29 mmol, 9 eq), and dibenzyl-*N*,*N*-diisopropyl phosphoramidite (559 mg, 1.62 mmol, 6 eq). Initially compound **26** was not soluble in the reaction mixture but after a couple hours it became solubilized. The reaction mixture was left to stir at room temperature for 16 hr. The reaction mixture was then cooled to -10°C. *m*-CPBA (395 mg, 2.29 mmol, 7 eq) was added to the reaction mixture portion-wise while stirring. The reaction mixture was then allowed to run for 15 minutes at room temperature. The reaction was diluted with DCM and washed with 10% sodium sulfite 3 times. The 10% sodium sulfite was then backwashed with DCM. The DCM was dried with sodium sulfate, and the product was filtered and concentrated. The product was a yellow viscous oil with small white crystals. The product was purified twice, first via flash column chromatography (0, 2, 4, 6, 8% methanol/DCM). Fractions 28-32 indicated the presence of an impure product using a TLC with 6% methanol/DCM (R_f-value = 0.51). The product was then purified using a Strata C18-E solid phase extraction column. The column was washed with methanol and equilibrated with 75% acetonitrile/H_2O. The crude product was loaded onto the column in 75% acetonitrile/H_2O and the sample was run with 75, 85, 95, and 100% acetonitrile/H_2O. The product eluted in fractions 13-17, the fractions were lyophilized and compound **27** (1.16 g, 0.738 mmol, 99% yield) was a clear solid.

SMILES: O=P(OCC1=CC=CC=C1)(OCC2=CC=CC=C2)O[C@H]3[C@@H](OCC4=CC=CC=C4)[C@@H](OP(OCC5=CC=CC=C5)(OCC6=CC=CC=C6)=O)[C@H](OP(OCC7=CC=CC=C7)(OCC8=CC=CC=C8)=O)[C@@H](OP(OCC9=CC=CC=C9)(OCC%10=CC=CC=C%10)=O)[C@@H]3OP(OCC%11=CC=CC=C%11)(OCC%12=CC=CC=C%12)=O

^{1}H-NMR (500 MHz, $CDCl_3$): δ 7.32-7.21 (m, 55H, H_{Bn}), 5.11-4.94 (m, 22H, $BnCH_2OP$, H_4-H_6), 4.78 (s, 2H, $PhCH_2O$), 4.75 (br s, 1H, H_2), 4.41 (q, J = 9.83 Hz, 1H, H_5), 4.34 (t, J = 7.9 Hz, 2H, H_1-H_3).

^{31}P NMR (202 MHz, $CDCl_3$): δ -1.01 (1P), -1.35 (2P), -2.02 (2P).

^{13}C-NMR (126 MHz, $CDCl_3$): δ 128.57 (5C), 128.55 (5C), 128.50 (5C), 128.36 (5C), 128.33 (9C), 128.26 (3C), 128.20 (3C), 128.18 (2C), 128.15 (6C), 128.13 (5C), 128.06 (5C), 128.04 (5C), 127.96 (5C), 127.54 (1C), 127.42 (2C), 76.91 (buried 1C), 75.86 (1C), 75.51 (1C), 75.26 (1C), 75.19 (1C), 75.14 (1C), 75.10 (1C), 69.84 (1C), 69.79 (1C), 69.73 (1C), 69.68 (1C), 69.66 (1C), 69.62 (3C), 69.58 (2C).

MALDI-MS. Calculated for $C_{83}H_{83}NaO_{21}P_5$ [M+Na] 1593.40; found 1593.42, 1609.40.

^{1}H NMR spectrum is in agreement with the literature report.[50]

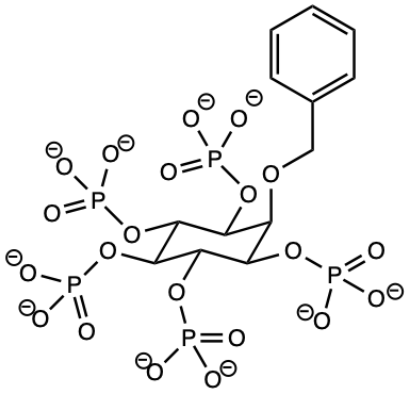

1,3,4,5,6-Phosphate-2-*O*-benzyl-*myo*-inositol (28)

Compound **27** (1571.42 g/mol, 0.318 mmol, 1 eq) was combined with *m*-cresol (108.14 g/mol, 195 mg, 37 eq) and thiophenol (110.18 g/mol, 1.851 mmol, 38 eq). The reaction mixture was cooled to 0°C and TFA (1.69 g, 14.805 mmol, 304 eq) was added. Next, bromotrimethylsilane (261 mg, 1.704 mmol, 35 eq) was added dropwise to the reaction mixture. The solution was stirred for 15 min at 0°C and then diluted in equal parts toluene and co-evaporated thrice. Distilled water was added to the crude product and it was separated with DCM thrice. The crude product was purified using a Strata C18-E solid phase extraction column. The column was washed with methanol and equilibrated with 0.1% TFA H_2O. The aqueous layer was loaded onto the column and the sample was run with 0.1% TFA/H_2O. The product eluted in fractions 2-4, the fractions were lyophilized and compound **28** was a white solid (132 mg, 0.197 mmol, 62% yield).

SMILES: C#CCO[C@H]1[C@@H](OP([O-])([O-])=O)[C@H](OP([O-])([O-])=O)[C@@H](OP([O-])([O-])=O)[C@H](OP([O-])([O-])=O)[C@H]1OP([O-])([O-])=O

^{1}H-NMR (400 MHz; D_2O): δ 7.40 (d, J = 7.08 Hz, 2H, H_{Bn}), 7.29 (t, J = 7.00 Hz, 2H, H_{Bn}), 7.24 (d, J = 7.16 Hz, 1H, H_{Bn}), 4.78 (s, 2H, Bn-CH_2), 4.44 (t, J = 8 Hz, 2H, H_4-H_6), 4.35 (t, J = 2.56 Hz, 1H, H_2), 4.3-4.23 (m, 3H, H_1-H_3-H_5).

^{31}P-NMR (202 MHz; D_2O): δ 0.26 (1P), -0.08 (2P), -0.79 (2P).

^{13}C-NMR (126 MHz; D_2O): δ 128.64 (3C), 128.38 (3C), 128.16 (1C), 46.64 (3C), 8.19 (3C).

HRMS FTMS E$^+$. Calculated for $C_{13}H_{22}O_{21}P_5^-$ [M-H] 668.93; found 668.9.

Experimental Procedures

Extent Cleavage Assay

TcdB extent cleavage induced by IP6 analogs was determined via the extent cleavage assay as previously reported, with some modifications.[20] In a 1.5 mL microcentrifuge tube Tris Buffer (100 mM Tris, 1 mM TCEP, pH 7.4) was combined individually with 50 μM of IP6 and each IP6 analog (IT1S5, IS5T1, IT2S4, IT3S3, IS3T3, IT6). For the experiments performed in the presence of divalent cation, $CaCl_2$, $MgCl_2$, or $ZnCl_2$ was added to the tubes containing IP6 analogs to get the final concentrations of 3 mM, 10 mM, 1.25 mM, 10 mM, 20 μM, or 100 μM. A negative control of no IP6 analog and a positive control of 1 mM IP6, corresponding to minimal and maximal toxin cleavage respectively, were included in every experiment. The tubes were equilibrated on a thermal shaker (MBI Lab Equipment) at 37ºC for 15 min at 300 rpm. 200 ng of TcdB (abcam, ab124001) was added to the 1.5 mL microcentrifuge tubes and the samples were shaken at 300 rpm at 37ºC for 3 hr. The assay was stopped upon addition of Laemmli sample buffer (LBx4), and the samples were boiled for 5 min. Samples were stored at -20ºC. The toxin cleavage products were separated by SDS-PAGE using a hand cast 8% acrylamide gel and MOPS SDS running buffer. The SDS-PAGE results were visualized using a modified version of the Vorum silver stain protocol and imaged on an Amersham Imager 600 (GE Healthcare).[51] The band intensities of the gels were quantified using ImageJ and the molar extent of cleavage (EoC) was calculated using the following formula:

$$\text{EoC (\%)} = \frac{\left(\frac{I_{207}}{207}\right)}{\left(\frac{I_{207}}{207}+\frac{I_{270}}{270}\right)} \text{ x } 100 \quad (1)$$

The EoC values were then normalized to the internal references for maximum (positive control) and minimum (negative control) cleavage:

$$\text{EoC}_{\text{norm}} = \frac{(\text{EoC} - \text{EoC}_{\text{min}})}{(\text{EoC}_{\text{max}} - \text{EoC}_{\text{min}})} \quad (2)$$

The EoC_{norm} of each IP6 analog was compared in Prism 10 (GraphPad) using Tukey's MCT, $p \leq 0.05$, $n = 15$.

Precipitation Assay

The precipitation of IP6 analogs in a simplified GI tract environment was determined via a modified turbidimetric precipitation assay.[52] To determine a qualitative assessment of precipitation, 250 μM of the ligand of interest (IP6, IS5T1, IT2S4, IT3S3, IT6, and EDTA) was combined with 100 mM of varied buffers at a pH of 2, 3, 4, 5, 6, 7, or 8. The buffers used were chloride, citrate, acetate, MES, HEPES, and Bis Tris. Each buffer was combined with either 3 mM or 10 mM $CaCl_2$, 1.25 mM or 10 mM $MgCl_2$, or 20 μM or 100 μM $ZnCl_2$, in a 96 well plate (Thermo Scientific, Nunclon Delta Surface) to achieve a final volume of 350 μL. The plate was rocked at room temperature for 30 min. The absorbance of each well was measured at 275 nm using a plate reader (Tecan Spark 10M Multimode Plate Reader) to determine the optical density (OD) of each well. The wavelength of 275 nm was determined experimentally based on the precipitate particle size.

Each OD readout was subtracted from its respective control OD (buffer with 250 μM of the ligand of interest), as none of the IP6 analogs absorb UV light. Next, OD was set relative to maximal OD, which was the highest observed OD value that could be induced by any of the small molecules (0.8083 AU induced by 250 μM IP6 in 10 mM $MgCl_2$, pH 7). Finally, in Prism 10 the average relative OD was plotted in a heat map with "1" as maximal precipitation and "0" as no observed precipitation. The OD for each experimental condition was compared to zero with a Wilcoxon t-test, $p \leq 0.001$, $n = 4$. To note, a significant p-value corresponded with visible white precipitate in the 96 well plate, except for the false positive reported for EDTA in 10 mM $CaCl_2$ at pH 8.

Chelation Assay

The amount of free $CaCl_2$ and $MgCl_2$ in the presence of the IP6 analogs was determined using a modified colorimetric assay protocol.[20] First, a standard curve was determined for $CaCl_2$ and $MgCl_2$ (500 nM – 1.6 mM) with 500 μM calmagite in 20 mM tris. The experiment was performed in a 96 well plate (Thermo Scientific, Nunclon Delta Surface) and the absorbance of Ca^{2+} and Mg^{2+} was measured with a plate reader (Tecan Spark 10M Multimode Plate Reader) at 550 and 539 nm, respectively.[53] The absorbance of calmagite alone subtracted from the absorbance with varied divalent cation concentrations was plotted against $CaCl_2$ and $MgCl_2$ concentration (log(M)), $n = 4$. The linear region of the corresponding semilog plot was fit with a

semilog linear regression in Prism 10 to yield the slopes 0.08722 and 0.06308 for $CaCl_2$ and $MgCl_2$, respectively. Next, the colorimetric assay was performed with 200 µM of IT1S5, IT2S4, IT3S3, and IT6, 500 µM calmagite, and either 200 µM of $CaCl_2$ or $MgCl_2$. The absorbance of Ca^{2+} and Mg^{2+} was measured, then subtracted from the absorbance of calmagite alone. The absorbance values were interpolated using the standard curve, giving the concentration of free divalent cation present in each sample. The amount of free Ca^{2+} and Mg^{2+} was compared in Prism 10 with a Tukey's MCT, $p \leq 0.05$, $n = 8$. The correlation between number of thiophosphates and amount of free Ca^{2+} was quantified via a simple linear regression (r), $p \leq 0.05$, $n = 8$.

Expression of the Truncated Cysteine Protease Domain

To generate the truncated cysteine protease domain (tCPD) from TcdB (TcdB 543-799 His6), the nucleotide sequence coding for amino acids 543—799 of TcdB was used. The pET22b-$TcdB_{543-799}$ plasmid was kindly donated by Dr. Matthew Bogyo and Dr. Aimee Shen, Stanford University. The plasmid was transformed into *Escherichia coli* BL21(DE3) by standard techniques. Overnight cultures of transformed BL21(DE3) were diluted 1:100 in 2 L Terrific Broth and grown at 37ºC until an OD_{600} of 0.8—0.9 was reached. IPTG was added and the cultures were grown for 3.5 hr at 30ºC. The cultures were pelleted by centrifugation at 5,000 x *g* for 30 min at 4ºC (Beckman J2-21, JS5.3). The cell pellets were resuspended in sonication buffer (20 mM phosphate, 100 mM NaCl, 1 mM $MgCl_2$, pH 8). The cell lysates were shaken for 30 min at 4ºC and then sonicated with a probe sonicator (Misonix Sonicator 3000). The cells were centrifuged at 5,000 x *g* for 30 min at 4ºC, then the supernatant was collected. tCPD was purified from the cleared lysate by metal-ion affinity chromatography using Co-NTA resin (ThermoFisher Scientific) at 4ºC. Eluted fractions containing protein were placed on a size exclusion gel filtration column (Superdex 75 HiLoad Prep column) at 4ºC and eluted into the desired buffer.

Crystallization and Structure Determination

Crystallization

The crystallization of tCPD was performed as previously described in the literature.[21] For tCPD bound to IP6, crystal hits were observed in 0.1 M tris HCl, pH 8.2, 36% (w/v) PEG2000 monomethyl ether as the precipitant. Diffraction quality crystals were grown at 22°C using the

sitting-drop vapor-diffusion method by mixing 1 mM of tCPD and 2 mM IP6 in 10 mM tris HCl, 150 mM NaCl, pH 7.5 with an equal volume of mother liquor and allowing the crystals to grow for 54-70 days.

Structure Determination

Diffraction data for both structures were collected on the CMCF-08ID-1 beamline at the Canadian Light Source. 1800 images were collected with an oscillation angle of 0.2° at 0.95371Å wavelength. Reflections were processed with autoPROC,[54] merged, and scaled with Aimless.[55] The structures were solved by molecular replacement using the structure of IHP-bound TcdB cysteine protease domain (PDB 3PEE) with PHASER[56] and refined with the Phenix suite[57] and Buster.[58] Models were built with Coot.[59] Data collection and refinement statistics are given in Table 4. The structure was deposited to the Protein Data Bank (code 9BJA).

Table 4. X-ray crystallography data collection and refinement statistics.

	TcdB: IP6 (PDB 9BJA)
	Crystal Parameter
Wavelength (Å)	0.95371
Resolution range (Å)	89.17–2.1 (2.16–2.1)
Space group	$P12_1$
Unit cell dimensions (Å)	44.051 89.171 67.597
Unit cell angles (deg)	90 103.782 90
Total reflections	199,044 (2,573)
Unique reflections	29,657 (403)
Multiplicity	6.7 (6.29)
Completeness (%)	99.9 (99.5)
Mean I/sigma(I)	9.3 (18.1)
Wilson B-factor	33.8
R-merge	0.106 (0.545)
$CC_{1/2}$	0.996 (0.911)
Reflections used for R-free	1496
R-work	0.2296
R-free	0.2574
# non-hydrogen atoms	4220
Macromolecules	3949
Ligands	72
Water	199
Protein residues	417
RMS (bonds, Å)	1.209
Ramachandran favored (%)	99

Ramachandran allowed (%)	1
Ramachandran outliers (%)	0
Clashscore	8.06
Average B-factor	44
Macromolecules	73
Ligands	32
Solvent	43.2

K_D Determination by ITC

ITC measurements were performed on the MicroCal iTC200 (Malvern Panalytical). All samples were prepared in a 10 mM tris buffer, 150 mM NaCl, 1 mM TCEP, pH 7.5. The sample cell contained 280 µL of 53 µM tCPD in the tris buffer. Protein used for this experiment was prepared the same day due to protein instability. A total of 39 µL of 530 µM IP6 analog in tris buffer was titrated into the sample cell with 29 successive injections at 10ºC. All samples were degassed and thermostated prior to measurements. Heat of dilution (HOD) runs were measured by injecting 530 µM IP6 analog into tris buffer alone. HOD measurements were subtracted from the corresponding thermal peaks measured for the sample prior to data analysis. The resulting differential binding heat data were analyzed with the MicroCal ORIGIN software using the one site model fitting. Errors were derived from fitting statistics.

EC_{50} Determination by Western Blotting

Extent Cleavage Assay

The experiment was followed similarily to what was described earlier, with some modifications. In a 1.5 mL microcentrifuge tube 10X bicarbonate buffer, pH 7.4, 10 mM TCEP, and a serial dilution of IP6, IT2S4, IT3S3, and IT6 were combined in either the absence or presence of divalent cations (1 mM $CaCl_2$, 150 µM $MgCl_2$, 12 µM $ZnCl_2$) and equilibrated in a thermal shaker (MBI Lab Equipment) at 300 rpm for 15 min at 37ºC. 500 pg of TcdB was added to the tubes and they were shaken at 300 rpm for 3 hr at 37ºC. The reaction was stopped with LBx4, and the samples were boiled for 5 min. Samples were stored at -20ºC. The toxin cleavage products were separated by SDS-PAGE using hand cast 8% acrylamide gels and MOPS SDS running buffer.

Western Blotting

The TcdB protein fragments were transferred onto a PVDF membrane at 100 V for 1.25 hr (BioRad, 1620177). Membranes were blocked with EveryBlot Blocking Buffer (BioRad, 12010020) for 30 min at room temperature. Membranes were then incubated on a rocking platform overnight at 4ºC with primary antibody against TcdB-GTD (R&D Systems, AF6246, 1:1000). The membranes were incubated for one hour at room temperature with Rabbit Anti-Sheep IgG H&L (Abcam, ab6746, 1:1000). The membranes were incubated for one hour at room temperature with Streptavidin (Abcam, ab7403, 1:5000). Between incubations the membrane was rinsed with TBST (1X Tris-Buffered Saline, 0.1% Tween 20 Detergent). Detection of protein levels was determined using enhanced chemiluminescence (Pierce ECL Western Blotting Substrate) and the signals were captured using an Amersham Imaging System (GE Healthcare). Densitometric analysis was performed using ImageJ Software.

Data Analysis

The extent cleavage of each experimental condition was determined as described earlier, with a modification. The EoC was calculated using the formula:

$$\text{EoC (\%)} = \frac{(I_{207})}{(I_{207}+I_{270})} \text{ x } 100 \quad (3)$$

The extent cleavage for each IP6 analog was then plotted against the logarithm of the concentration of IP6 analog. The resultant plot was fit with a nonlinear curve fit in Prism 10 (Variable slope, 4 parameters); the corresponding median effective concentration (EC_{50}) and SD's were reported, n = 6.

Protonation Assay

All ITC measurements were performed on the MicroCal VP iTC. All samples were prepared in 50 mM buffer, 1 mM TCEP, I = 150 mM, pH 7.5.

$$I = 0.5\sum(c * z^2) \quad (4)$$

Where, c = concentration, z = charge.

The buffers used were phosphate, HEPES, imidazole, and tris. Protein used for this experiment was prepared the same day due to protein instability. The sample cell contained 2 mL of 53 µM

tCPD in the respective buffer for that experiment. A total of 1.4 mL of 530 μM IP6 analog in the respective buffer for the experiment was titrated into the sample cell with 29 successive injections at 25ºC. All samples were degassed and thermostated prior to measurements. HOD was measured by injecting 530 μM IP6 analog solution into buffer alone. HOD was subtracted from the corresponding thermal peaks measured for the sample prior to data analysis. The resulting differential binding heat data was analyzed with the MicroCal ORIGIN software using the one site model fitting.

The enthalpy of each binding interaction (ΔH^{o}_{obs}) in every respective buffer was plotted against the corresponding ionization enthalpy of the buffer (ΔH^{b}_{i}).[60] A linear fit was performed in Prism 10 for each IP6 analog dataset. A one sample t-test was performed with the slope of each line and zero ($p \leq 0.05$). This analysis was performed in OriginPro software.

$$\Delta H^{o}_{obs} = \Delta H^{o}_{0} + N_{H+}\Delta H^{b}_{i} \quad (5)$$

ΔH^{o}_{0} is the enthalpy that would be measured if the ionization enthalpy of the buffer were equal to zero, and N_{H+} is the change in number of bound protons.[45]

pK Determination

IP6 and IT6 in their sodium form were converted to their protonated form as described previously.[61] The protonated compounds were titrated with 50 mM tetrabutylammonium hydroxide (NBu_4OH) to the desired pH, as described previously.[22] pH measurements were taken from ~ 4 – 10 to assess the physiologically relevant pK's. pH was measured with a benchtop laboratory pH/mV meter (Fisher brand accumet Basic AB315) and a glass electrode. The pH meter was cleaned (Thermo Scientific, Orion pH electrode cleaning solution) and calibrated (Thermo Scientific, Orion Application Solution) prior to each use. When the desired pH was achieved a 600 μL aliquot containing 4 mM IP6 or IT6, NBu_4OH, and 4 mM trimethyl phosphate in 10% D_2O was placed in an 8 in, 5 mm O.D. NMR tube (Fisher Scientific). A ^{31}P NMR with ^{1}H coupling was performed on an AVIIIHD 500 MHz Bruker NMR. The ^{31}P-{^{1}H} chemical shifts were measured relative to trimethyl phosphate (TMP), the internal reference. Phosphorus peak assignment was made in accordance with literature.[22] NMR experiments were conducted at 300 K.

Detected pH was plotted against ^{31}P-{^{1}H} chemical shifts. Protonation constants were calculated by fitting the titration curves with an asymmetric sigmoidal non-linear curve fit in Prism 10. The inflection points of the curve fit were reported as the apparent pK's for each functional group on IP6 and IT6. Values were reported as mean ± SD, n = 3.

Differential Scanning Fluorometry

Differential Scanning Fluorometry was performed with tCPD at a final concentration of 0.4 µg/µL in 50 mM tris, I = 150 mM, 1 mM TCEP, pH 7.5, was combined with 4X SYPRO Orange, and a serial dilution of IP6, IT1S5, IT2S4, IT3S3, and IT6. Protein used for this experiment was prepared the same day due to protein instability. A CFX Connect Real-Time System qRT-PCR thermocycler (Bio-Rad) was used to establish a temperature gradient from 25ºC to 95ºC in 0.2ºC increments, while simultaneously recording the increase in SYPRO Orange fluorescence over 10 sec. The Bio-Rad CFX Connect Manager software was used to integrate the fluorescence curves to calculate the melting temperature (T_M). The T_M for each IP6 analog was then plotted against the logarithm of the concentration of IP6 analog. The resultant plot was fit with a nonlinear curve fit in Prism 10 (Variable slope, 4 parameters), the A2 value was used to determine the maximum change in T_M induced by the presence of IP6 analogs.

Protein NMR

HSQC

^{1}H-^{15}N-HSQC NMR data were acquired on a Bruker AVIIIHD 800 MHz NMR Spectrometer equipped with a TCI cryoprobe at 300 K in pH 7.5 buffer containing 25 mM tris, 100 mM NaCl, 1 mM TCEP, 10% D_2O. Proteins were uniformly enriched with ^{15}N, as described previously.[62] Protein used for this experiment was prepared the same day due to protein instability. D_2O was used as an internal reference for spectral calibration. NMR spectra were processed using Topspin 4.3.0 and analyzed with POKY.[63] Spectral peak assignment did not correspond with amino acid number as a full NMR characterization of tCPD was not performed. Instead, the HSQC with the greatest number of peaks was assigned in order from 1 to 208, where 1 was the peak with the lowest ppm on the ^{1}H spectrum and 208 was the peak with the highest ppm. The remaining spectra were assigned by overlapping with the original assigned spectra, and the closest peaks to those from the assigned spectra were given the same number. To investigate peak-specific

structural perturbations due to ligand induced changes in tCPD, chemical shift perturbations (CSPs) were calculated using the equation:

$$CSP = \sqrt{(\Delta\delta H_N)^2 + (0.1\Delta\delta N_H)^2} \quad (6)$$

Where $\Delta\ \delta H_N$ and δN_H are the difference in the chemical shift of proton and nitrogen, respectively.[47] The threshold (θ) of significance was the average of all CSP values plus two SD (95%) for two independent spectra of the holo-protein bound to a molar equivalent of ligand. HSQC spectra were collected for 350 μM uniformly ^{15}N-labeled protein samples with 141 - 208 data points (number of data points varied between samples) and with 4 scans.

Phosphorus NMR

^{31}P NMR data were acquired on a Bruker AVIIIHD 500 MHz NMR Spectrometer with a HX (X = ^{109}Ag-^{19}F) probe. All samples prepared for the ^{1}H-^{15}N-HSQC NMR data were also used for ^{31}P NMR tracking to determine whether IP6 or IT3S3 was bound to tCPD in a competition assay. ^{31}P spectra had ^{1}H-decoupling and were collected at 300 K with 512 scans.

Statistical Analysis

All statistical tests were proceeded by a Shapiro-Wilk test to test for normality. Statistics for each experiment were based on whether the raw data were normally distributed.

ASSOCIATED CONTENT

Supporting Information

Additional figures containing the colorimetric assay standard curve, ITC raw datasets, extent cleavage data for IP5Bn, pK determination raw datasets, supplementary ^{1}H-^{15}N HSQC results, ^{31}P NMR reaction tracking of the HSQC experiment, all silver-stained gels and western blot membranes, and all NMR's of the characterized compounds can be found in "Supporting Information".

Accession Codes

PDB code for tCPD bound to IP6 is 9BJA.

AUTHOR INFORMATION

Corresponding Author

*E-mail: bastien.castagner@mcgill.ca. Phone: 514-398-2181. Fax: 514-398-2045.

Present/Current Author Addresses

1 NuChem Sciences Inc., 480 Rue Perreault, Lévis, QC, Canada.

Notes

B.C. is co-inventor of patents WO2013045107A1 and WO2017098033A1 licensed to CSL Vifor. The remaining authors declare no competing interests.

ACKNOWLEDGEMENTS

We would like to gratefully acknowledge Dr. Matthew Bogyo and Dr. Aimee Shen for providing the $tCPD_{544\text{-}797}$ plasmid. We also acknowledge Dr. Kim Munro and the Centre for Structural Biology Research (CRBS), supported by the *Fond de Recherche du Québec – Santé* (FRQS), for use of the core facilities. NMR experiments were recorded at the Québec/Eastern Canada High Field NMR Facility, supported by the Canada Foundation for Innovation, McGill University Faculty of Science and Department of Chemistry. We also acknowledge Dr. Tara Sprules for assistance with the NMR experiments. Mass Spectrometry was performed by the McGill Chemistry Characterization Mass Spectrometry facility. Funding for this project was provided by a Canadian Institutes of Health Research (CIHR) project grant (PJT-173262) to Dr. Bastien Castagner and Dr. Jean-Francois Trempe and a Natural Science and Engineering Research council of Canada (NSERC) discovery grant (RGPIN-2020-04908) to Dr. Castagner. Dr. Castagner is a tier 2 Canada Research Chair (CRC) in Therapeutic Chemistry and Dr. Trempe is a tier 2 CRC in Structural Pharmacology.

ABBREVIATIONS USED

CDI, *Clostridioides difficile* infection; CDC, Centers for Disease Control and Prevention; TcdA, Toxin A; TcdB, Toxin B; CPD, Cysteine protease domain; GTD, Glucosyltransferase domain; FDA, Food and Drug Administration; IP6, Inositol hexakisphosphate; IT1S5, 5-(*O*-thiophosphate)-*myo*-inositol-1,2,3,4,6-penta-*O*-sulfate (**12**); IS5T1, 2-(*O*-thiophosphate)-*myo*-inositol-1,3,4,5,6-penta-*O*-sulfate (**8**); IT2S4, 4,6-(di-*O*-thiophosphate)-*myo*-inositol-1,2,3,5-tetra-*O*-sulfate[20]; IT3S3, 1,3,5-(tri-*O*-thiophosphate)-*myo*-inositol-2,4,6-tri-*O*-sulfate (**16**);

IS3T3, 2,4,6-(tri-*O*-thiophosphate)-*myo*-inositol-1,3,5-tri-*O*-sulfate (**21**); IT6, hexakis-thiophosphate (**23**); SAR, Structure Activity Relationship; tCPD, truncated cysteine protease domain; GI, gastrointestinal; DMF, Dimethylformamide; DIBAL-H, Diisobutylaluminum hydride; NBu_4OH , tetrabutylammonium hydroxide; IS6, myo-inositol hexasulfate; EDTA, ethylenediamine tetraacetic acid; OD, Optical Density; MCT, multiple comparisons test; K_D, dissociation constant; ITC, isothermal calorimetry; EC_{50}, effective median concentration; IP5Bn, 1,3,4,5,6-phosphate-2-*O*-benzyl-*myo*-inositol; DSF, differential scanning fluorimetry; T_M, melting temperature; ΔT_M, change in melting temperature; HSQC, heteronuclear single quantum coherence spectroscopy; CSP, chemical shift perturbation; s, singlet; d, doublet; t, triplet; q, quartet; sept, septet; dd, doublet-doublet; dt, doublet-triplet; dq, doublet-quartet; td, triplet-doublet; m, multiplet; br s, broad signal.

REFERENCES

(1) Loo, V. G.; Poirier, L.; Miller, M. A.; Oughton, M.; Libman, M. D.; Michaud, S.; Bourgault, A.-M.; Nguyen, T.; Frenette, C.; Kelly, M.; Vibien, A.; Brassard, P.; Fenn, S.; Dewar, K.; Hudson, T. J.; Horn, R.; René, P.; Monczak, Y.; Dascal, A. A Predominantly Clonal Multi-Institutional Outbreak of *Clostridium Difficile* –Associated Diarrhea with High Morbidity and Mortality. *N. Engl. J. Med.* **2005**, *353* (23), 2442–2449. https://doi.org/10.1056/NEJMoa051639.

(2) Slimings, C.; Riley, T. V. Antibiotics and Hospital-Acquired Clostridium Difficile Infection: Update of Systematic Review and Meta-Analysis. *J. Antimicrob. Chemother.* **2014**, *69* (4), 881–891. https://doi.org/10.1093/jac/dkt477.

(3) Centers for Disease Control and Prevention (U.S.). *Antibiotic Resistance Threats in the United States, 2019*; Centers for Disease Control and Prevention (U.S.), 2019. https://doi.org/10.15620/cdc:82532.

(4) Deshpande, A.; Pasupuleti, V.; Thota, P.; Pant, C.; Rolston, D. D. K.; Hernandez, A. V.; Donskey, C. J.; Fraser, T. G. Risk Factors for Recurrent *Clostridium Difficile* Infection: A Systematic Review and Meta-Analysis. *Infect. Control Hosp. Epidemiol.* **2015**, *36* (4), 452–460. https://doi.org/10.1017/ice.2014.88.

(5) Dickey, S. W.; Cheung, G. Y. C.; Otto, M. Different Drugs for Bad Bugs: Antivirulence Strategies in the Age of Antibiotic Resistance. *Nat. Rev. Drug Discov.* **2017**, *16* (7), 457–471. https://doi.org/10.1038/nrd.2017.23.

(6) Kordus, S. L.; Thomas, A. K.; Lacy, D. B. Clostridioides Difficile Toxins: Mechanisms of Action and Antitoxin Therapeutics. *Nat. Rev. Microbiol.* **2022**, *20* (5), 285–298. https://doi.org/10.1038/s41579-021-00660-2.

(7) Orrell, K. E.; Melnyk, R. A. Large Clostridial Toxins: Mechanisms and Roles in Disease. *Microbiol. Mol. Biol. Rev. MMBR* **2021**, *85* (3), e0006421. https://doi.org/10.1128/MMBR.00064-21.

(8) Wilcox, M. H.; Gerding, D. N.; Poxton, I. R.; Kelly, C.; Nathan, R.; Birch, T.; Cornely, O. A.; Rahav, G.; Bouza, E.; Lee, C.; Jenkin, G.; Jensen, W.; Kim, Y.-S.; Yoshida, J.;

Gabryelski, L.; Pedley, A.; Eves, K.; Tipping, R.; Guris, D.; Kartsonis, N.; Dorr, M.-B. Bezlotoxumab for Prevention of Recurrent *Clostridium Difficile* Infection. *N. Engl. J. Med.* **2017**, *376* (4), 305–317. https://doi.org/10.1056/NEJMoa1602615.

(9) Lyras, D.; O'Connor, J. R.; Howarth, P. M.; Sambol, S. P.; Carter, G. P.; Phumoonna, T.; Poon, R.; Adams, V.; Vedantam, G.; Johnson, S.; Gerding, D. N.; Rood, J. I. Toxin B Is Essential for Virulence of Clostridium Difficile. *Nature* **2009**, *458* (7242), 1176–1179. https://doi.org/10.1038/nature07822.

(10) Carter, G. P.; Chakravorty, A.; Pham Nguyen, T. A.; Mileto, S.; Schreiber, F.; Li, L.; Howarth, P.; Clare, S.; Cunningham, B.; Sambol, S. P.; Cheknis, A.; Figueroa, I.; Johnson, S.; Gerding, D.; Rood, J. I.; Dougan, G.; Lawley, T. D.; Lyras, D. Defining the Roles of TcdA and TcdB in Localized Gastrointestinal Disease, Systemic Organ Damage, and the Host Response during Clostridium Difficile Infections. *mBio* **2015**, *6* (3), 10.1128/mbio.00551-15. https://doi.org/10.1128/mbio.00551-15.

(11) Jiang, M.; Shin, J.; Simeon, R.; Chang, J.-Y.; Meng, R.; Wang, Y.; Shinde, O.; Li, P.; Chen, Z.; Zhang, J. Structural Dynamics of Receptor Recognition and pH-Induced Dissociation of Full-Length Clostridioides Difficile Toxin B. *PLOS Biol.* **2022**, *20* (3), e3001589. https://doi.org/10.1371/journal.pbio.3001589.

(12) Orrell, K. E.; Mansfield, M. J.; Doxey, A. C.; Melnyk, R. A. The C. Difficile Toxin B Membrane Translocation Machinery Is an Evolutionarily Conserved Protein Delivery Apparatus. *Nat. Commun.* **2020**, *11* (1), 432. https://doi.org/10.1038/s41467-020-14306-z.

(13) Just, I.; Selzer, J.; Wilm, M.; Eichel-Streiber, C. V.; Mann, M.; Aktories, K. Glucosylation of Rho Proteins by Clostridium Difficile Toxin B. *Nature* **1995**, *375* (6531), 500–503. https://doi.org/10.1038/375500a0.

(14) Giacobbe, D. R.; Dettori, S.; Di Bella, S.; Vena, A.; Granata, G.; Luzzati, R.; Petrosillo, N.; Bassetti, M. Bezlotoxumab for Preventing Recurrent Clostridioides Difficile Infection: A Narrative Review from Pathophysiology to Clinical Studies. *Infect. Dis. Ther.* **2020**, *9* (3), 481–494. https://doi.org/10.1007/s40121-020-00314-5.

(15) Stroke, I. L.; Letourneau, J. J.; Miller, T. E.; Xu, Y.; Pechik, I.; Savoly, D. R.; Ma, L.; Sturzenbecker, L. J.; Sabalski, J.; Stein, P. D.; Webb, M. L.; Hilbert, D. W. Treatment of Clostridium Difficile Infection with a Small-Molecule Inhibitor of Toxin UDP-Glucose Hydrolysis Activity. *Antimicrob. Agents Chemother.* **2018**, *62* (5), e00107-18. https://doi.org/10.1128/AAC.00107-18.

(16) Tam, J.; Hamza, T.; Ma, B.; Chen, K.; Beilhartz, G. L.; Ravel, J.; Feng, H.; Melnyk, R. A. Host-Targeted Niclosamide Inhibits C. Difficile Virulence and Prevents Disease in Mice without Disrupting the Gut Microbiota. *Nat. Commun.* **2018**, *9* (1), 5233. https://doi.org/10.1038/s41467-018-07705-w.

(17) Puri, A. W.; Lupardus, P. J.; Deu, E.; Albrow, V. E.; Garcia, K. C.; Bogyo, M.; Shen, A. Rational Design of Inhibitors and Activity-Based Probes Targeting Clostridium Difficile Virulence Factor TcdB. *Chem. Biol.* **2010**, *17* (11), 1201–1211. https://doi.org/10.1016/j.chembiol.2010.09.011.

(18) Savidge, T. C.; Urvil, P.; Oezguen, N.; Ali, K.; Choudhury, A.; Acharya, V.; Pinchuk, I.; Torres, A. G.; English, R. D.; Wiktorowicz, J. E.; Loeffelholz, M.; Kumar, R.; Shi, L.; Nie, W.; Braun, W.; Herman, B.; Hausladen, A.; Feng, H.; Stamler, J. S.; Pothoulakis, C. Host S-Nitrosylation Inhibits Clostridial Small Molecule–Activated Glucosylating Toxins. *Nat. Med.* **2011**, *17* (9), 1136–1141. https://doi.org/10.1038/nm.2405.

(19) Paparella, A. S.; Aboulache, B. L.; Harijan, R. K.; Potts, K. S.; Tyler, P. C.; Schramm, V. L. Inhibition of Clostridium Difficile TcdA and TcdB Toxins with Transition State Analogues. *Nat. Commun.* **2021**, *12* (1), 6285. https://doi.org/10.1038/s41467-021-26580-6.
(20) Ivarsson, M. E.; Durantie, E.; Huberli, C.; Huwiler, S.; Hegde, C.; Friedman, J.; Altamura, F.; Lu, J.; Verdu, E. F.; Bercik, P.; Logan, S. M.; Chen, W.; Leroux, J.-C.; Castagner, B. Small-Molecule Allosteric Triggers of Clostridium Difficile Toxin B Auto-Proteolysis as a Therapeutic Strategy. *Cell Chem. Biol.* **2019**, *26* (1), 17-26.e13. https://doi.org/10.1016/j.chembiol.2018.10.002.
(21) Shen, A.; Lupardus, P. J.; Gersch, M. M.; Puri, A. W.; Albrow, V. E.; Garcia, K. C.; Bogyo, M. Defining an Allosteric Circuit in the Cysteine Protease Domain of Clostridium Difficile Toxins. *Nat. Struct. Mol. Biol.* **2011**, *18* (3), 364–371. https://doi.org/10.1038/nsmb.1990.
(22) Costello, A. J. R.; Glonek, T.; Myers, T. C. 31P Nuclear Magnetic resonance□pH Titrations of Myo-Inositol Hexaphosphate. *Carbohydr. Res.* **1976**, *46* (2), 159–171. https://doi.org/10.1016/S0008-6215(00)84287-1.
(23) Maenz, D.; Engele-Schaan, C.; Newkirk, R.; Classen, H. The Effect of Minerals and Mineral Chelators on the Formation of Phytase-Resistant and Phytase-Susceptible Forms of Phytic Acid in a Slurry of Canola Meal. *Anim. Feed Sci. Technol.* **1999**, *81*, 177–192.
(24) Akond, A. S. M. G. M.; Crawford, H.; Berthold, J.; Talukder, Z. I.; Hossain, K. Minerals (Zn, Fe, Ca and Mg) and Antinutrient (Phytic Acid) Constituents in Common Bean. *Am. J. Food Technol.* **2011**, *6* (3), 235–243. https://doi.org/10.3923/ajft.2011.235.243.
(25) Lopez, H. W.; Leenhardt, F.; Coudray, C.; Remesy, C. Minerals and Phytic Acid Interactions: Is It a Real Problem for Human Nutrition? *Int. J. Food Sci. Technol.* **2002**, *37* (7), 727–739. https://doi.org/10.1046/j.1365-2621.2002.00618.x.
(26) Haros, M.; Carlsson, N.-G.; Almgren, A.; Larsson-Alminger, M.; Sandberg, A.-S.; Andlid, T. Phytate Degradation by Human Gut Isolated Bifidobacterium Pseudocatenulatum ATCC27919 and Its Probiotic Potential. *Int. J. Food Microbiol.* **2009**, *135* (1), 7–14. https://doi.org/10.1016/j.ijfoodmicro.2009.07.015.
(27) Novotná, B.; Vaneková, L.; Zavřel, M.; Buděšínský, M.; Dejmek, M.; Smola, M.; Gutten, O.; Tehrani, Z. A.; Pimková Polidarová, M.; Brázdová, A.; Liboska, R.; Štěpánek, I.; Vavřina, Z.; Jandušík, T.; Nencka, R.; Rulíšek, L.; Bouřa, E.; Brynda, J.; Páv, O.; Birkuš, G. Enzymatic Preparation of 2′–5′,3′–5′-Cyclic Dinucleotides, Their Binding Properties to Stimulator of Interferon Genes Adaptor Protein, and Structure/Activity Correlations. *J. Med. Chem.* **2019**, *62* (23), 10676–10690. https://doi.org/10.1021/acs.jmedchem.9b01062.
(28) Zhao, Z. Thiophosphate Derivatives as Inhibitors of Tyrosine Phosphatases. *Biochem. Biophys. Res. Commun.* **1996**, *218* (2), 480–484. https://doi.org/10.1006/bbrc.1996.0085.
(29) Lee, H. W.; Kishi, Y. Synthesis of Mono- and Unsymmetrical Bis-Orthoesters of Scyllo-Inositol. *J. Org. Chem.* **1985**, *50* (22), 4402–4404. https://doi.org/10.1021/jo00222a046.
(30) Riley, A. M.; Guédat, P.; Schlewer, G.; Spiess, B.; Potter, B. V. L. A Conformationally Restricted Cyclic Phosphate Analogue of Inositol Trisphosphate: Synthesis and Physicochemical Properties. *J. Org. Chem.* **1998**, *63* (2), 295–305. https://doi.org/10.1021/jo9714425.
(31) Godage, H. Y.; Riley, A. M.; Woodman, T. J.; Thomas, M. P.; Mahon, M. F.; Potter, B. V. L. Regioselective Opening of *Myo* -Inositol Orthoesters: Mechanism and Synthetic Utility. *J. Org. Chem.* **2013**, *78* (6), 2275–2288. https://doi.org/10.1021/jo3027774.

(32) Billington, D. C.; Baker, R.; Kulagowski, J. J.; Mawer, I. M.; Vacca, J. P.; deSolms, S. J.; Huff, J. R. The Total Synthesis of Myo-Inositol Phosphates via Myo-Inositol Orthoformate. *J. Chem. Soc. Perkin 1* **1989**, No. 8, 1423. https://doi.org/10.1039/p19890001423.
(33) Murali, C.; Shashidhar, M. S.; Gopinath, C. S. Hydroxyl Group Deprotection Reactions with Pd(OH)2/C: A Convenient Alternative to Hydrogenolysis of Benzyl Ethers and Acid Hydrolysis of Ketals. *Tetrahedron* **2007**, *63* (19), 4149–4155. https://doi.org/10.1016/j.tet.2007.02.096.
(34) Mills, S. J.; Liu, C.; Potter, B. V. L. Synthesis of D- and l-Myo-Inositol 2,4,5-Trisphosphate and Trisphosphorothioate: Structural Analogues of d-Myo-Inositol 1,4,5-Trisphosphate. *Carbohydr. Res.* **2002**, *337* (20), 1795–1801. https://doi.org/10.1016/S0008-6215(02)00289-6.
(35) Chen, D.; Oezguen, N.; Urvil, P.; Ferguson, C.; Dann, S. M.; Savidge, T. C. Regulation of Protein-Ligand Binding Affinity by Hydrogen Bond Pairing. *Sci. Adv.* **2016**, *2* (3), e1501240. https://doi.org/10.1126/sciadv.1501240.
(36) Chen, P.; Lam, K.; Liu, Z.; Mindlin, F. A.; Chen, B.; Gutierrez, C. B.; Huang, L.; Zhang, Y.; Hamza, T.; Feng, H.; Matsui, T.; Bowen, M. E.; Perry, K.; Jin, R. Structure of the Full-Length Clostridium Difficile Toxin B. *Nat. Struct. Mol. Biol.* **2019**, *26* (8), 712–719. https://doi.org/10.1038/s41594-019-0268-0.
(37) Hoenderop, J. G. J.; Nilius, B.; Bindels, R. J. M. Calcium Absorption Across Epithelia. *Physiol. Rev.* **2005**, *85* (1), 373–422. https://doi.org/10.1152/physrev.00003.2004.
(38) Schweigel, M., M. Magnesium Transport in the Gastrointestinal Tract. *Front. Biosci.* **2000**, *5* (1), d666. https://doi.org/10.2741/Schweigel.
(39) Maares, M.; Haase, H. A Guide to Human Zinc Absorption: General Overview and Recent Advances of In Vitro Intestinal Models. *Nutrients* **2020**, *12* (3), 762. https://doi.org/10.3390/nu12030762.
(40) *Zinc in Human Biology*; Mills, C. F., Mills, C. F., Eds.; ILSI human nutrition reviews; Springer: London, 1989.
(41) Velazquez-Campoy, A.; Claro, B.; Abian, O.; Höring, J.; Bourlon, L.; Claveria-Gimeno, R.; Ennifar, E.; England, P.; Chaires, J. B.; Wu, D.; Piszczek, G.; Brautigam, C.; Tso, S.-C.; Zhao, H.; Schuck, P.; Keller, S.; Bastos, M. A Multi-Laboratory Benchmark Study of Isothermal Titration Calorimetry (ITC) Using Ca2+ and Mg2+ Binding to EDTA. *Eur. Biophys. J.* **2021**, *50* (3–4), 429–451. https://doi.org/10.1007/s00249-021-01523-7.
(42) Zhang, H.-J.; Ociepa, M.; Nassir, M.; Zheng, B.; Lewicki, S. A.; Salmaso, V.; Baburi, H.; Nagel, J.; Mirza, S.; Bueschbell, B.; Al-Hroub, H.; Perzanowska, O.; Lin, Z.; Schmidt, M. A.; Eastgate, M. D.; Jacobson, K. A.; Müller, C. E.; Kowalska, J.; Jemielity, J.; Baran, P. S. Stereocontrolled Access to Thioisosteres of Nucleoside Di- and Triphosphates. *Nat. Chem.* **2024**, *16* (2), 249–258. https://doi.org/10.1038/s41557-023-01347-2.
(43) Jaffe, E. K.; Cohn, M. ^{31} P Nuclear Magnetic Resonance Spectra of the Thiophosphate Analogs of Adenine Nucleotides; Effects of pH and Mg $^{2+}$ Binding. *Biochemistry* **1978**, *17* (4), 652–657. https://doi.org/10.1021/bi00597a014.
(44) Kalsin, A. M.; Kowalczyk, B.; Smoukov, S. K.; Klajn, R.; Grzybowski, B. A. Ionic-like Behavior of Oppositely Charged Nanoparticles. *J. Am. Chem. Soc.* **2006**, *128* (47), 15046–15047. https://doi.org/10.1021/ja0642966.
(45) Baker, B. M.; Murphy, K. P. Evaluation of Linked Protonation Effects in Protein Binding Reactions Using Isothermal Titration Calorimetry. *Biophys. J.* **1996**, *71* (4), 2049–2055. https://doi.org/10.1016/S0006-3495(96)79403-1.

(46) Onufriev, A. V.; Alexov, E. Protonation and pK Changes in Protein–Ligand Binding. *Q. Rev. Biophys.* **2013**, *46* (2), 181–209. https://doi.org/10.1017/S0033583513000024.
(47) Williamson, M. P. Using Chemical Shift Perturbation to Characterise Ligand Binding. *Prog. Nucl. Magn. Reson. Spectrosc.* **2013**, *73*, 1–16. https://doi.org/10.1016/j.pnmrs.2013.02.001.
(48) Lampe, D.; Liu, C.; Potter, B. V. L. Synthesis of Selective Non-Ca2+ Mobilizing Inhibitors of D-Myo-Inositol 1,4,5-Trisphosphate 5-Phosphatase. *J. Med. Chem.* **1994**, *37* (7), 907–912. https://doi.org/10.1021/jm00033a007.
(49) Zapata, A.; Fernandez De La Pradilla, R.; Martin-Lomas, M.; Penades, S. Novel Highly Regioselective O-Alkylation and O-Acylation of Myo-Inositol. *J. Org. Chem.* **1991**, *56* (1), 444–447. https://doi.org/10.1021/jo00001a085.
(50) Riley, A. M.; Trusselle, M.; Kuad, P.; Borkovec, M.; Cho, J.; Choi, J. H.; Qian, X.; Shears, S. B.; Spiess, B.; Potter, B. V. L. Scyllo-Inositol Pentakisphosphate as an Analogue of Myo-Inositol 1,3,4,5,6-Pentakisphosphate: Chemical Synthesis, Physicochemistry and Biological Applications. *ChemBioChem* **2006**, *7* (7), 1114–1122. https://doi.org/10.1002/cbic.200600037.
(51) Mortz, E.; Krogh, T. N.; Vorum, H.; Görg, A. Improved Silver Staining Protocols for High Sensitivity Protein Identification Using Matrix-Assisted Laser Desorption/Ionization-Time of Flight Analysis. *PROTEOMICS* **2001**, *1* (11), 1359–1363. https://doi.org/10.1002/1615-9861(200111)1:11<1359::AID-PROT1359>3.0.CO;2-Q.
(52) Mathieson, A. R. The Turbidimetric Precipitation Titration of Polystyrene. *J. Colloid Sci.* **1960**, *15* (5), 387–401. https://doi.org/10.1016/0095-8522(60)90043-X.
(53) Rasouli, Z.; Ghavami, R. Simultaneously Detection of Calcium and Magnesium in Various Samples by Calmagite and Chemometrics Data Processing. *Spectrochim. Acta. A. Mol. Biomol. Spectrosc.* **2016**, *169*, 72–81. https://doi.org/10.1016/j.saa.2016.06.027.
(54) Vonrhein, C.; Flensburg, C.; Keller, P.; Sharff, A.; Smart, O.; Paciorek, W.; Womack, T.; Bricogne, G. Data Processing and Analysis with the *autoPROC* Toolbox. *Acta Crystallogr. D Biol. Crystallogr.* **2011**, *67* (4), 293–302. https://doi.org/10.1107/S0907444911007773.
(55) Evans, P. R.; Murshudov, G. N. How Good Are My Data and What Is the Resolution? *Acta Crystallogr. D Biol. Crystallogr.* **2013**, *69* (7), 1204–1214. https://doi.org/10.1107/S0907444913000061.
(56) McCoy, A. J.; Grosse-Kunstleve, R. W.; Adams, P. D.; Winn, M. D.; Storoni, L. C.; Read, R. J. *Phaser* Crystallographic Software. *J. Appl. Crystallogr.* **2007**, *40* (4), 658–674. https://doi.org/10.1107/S0021889807021206.
(57) Liebschner, D.; Afonine, P. V.; Baker, M. L.; Bunkóczi, G.; Chen, V. B.; Croll, T. I.; Hintze, B.; Hung, L.-W.; Jain, S.; McCoy, A. J.; Moriarty, N. W.; Oeffner, R. D.; Poon, B. K.; Prisant, M. G.; Read, R. J.; Richardson, J. S.; Richardson, D. C.; Sammito, M. D.; Sobolev, O. V.; Stockwell, D. H.; Terwilliger, T. C.; Urzhumtsev, A. G.; Videau, L. L.; Williams, C. J.; Adams, P. D. Macromolecular Structure Determination Using X-Rays, Neutrons and Electrons: Recent Developments in *Phenix*. *Acta Crystallogr. Sect. Struct. Biol.* **2019**, *75* (10), 861–877. https://doi.org/10.1107/S2059798319011471.
(58) Bricogne, G.; Blanc, E.; Brandl, M.; Flensburg, C.; Keller, P.; Paciorek, W.; Roversi, P.; Sharff, A.; Smart, O.; Vonrhein, C.; Womack, T. BUSTER, 2017.
(59) Emsley, P.; Lohkamp, B.; Scott, W. G.; Cowtan, K. Features and Development of *Coot*. *Acta Crystallogr. D Biol. Crystallogr.* **2010**, *66* (4), 486–501. https://doi.org/10.1107/S0907444910007493.

(60) Christensen, J. J.; Hansen, L. D.; Izatt, R. M. *Handbook of Proton Ionization Heats and Related Thermodynamic Quantities*; Contribution from the Center for Thermochemical Studies, Brigham Young University, Provo, Utah; Wiley: New York, 1976.
(61) Brigando, C.; Mossoyan, J. C.; Favier, F.; Benlian, D. Conformational Preferences and Protonation Sequence of Myo-Lnositol Hexaphosphate in Aqueous Solution; Potentiometric and Multinuclear Magnetic Resonance Studies. *J CHEM SOC DALTON TRANS* **1995**.
(62) Marley, J.; Lu, M.; Bracken, C. A Method for Efficient Isotopic Labeling of Recombinant Proteins. *J. Biomol. NMR* **2001**, *20* (1), 71–75. https://doi.org/10.1023/A:1011254402785.
(63) Lee, W.; Rahimi, M.; Lee, Y.; Chiu, A. POKY: A Software Suite for Multidimensional NMR and 3D Structure Calculation of Biomolecules. *Bioinformatics* **2021**, *37* (18), 3041–3042. https://doi.org/10.1093/bioinformatics/btab180.